INFORMATION TO USERS

This manuscript has been reproduced from the microfilm master. UMI films the text directly from the original or copy submitted. Thus, some thesis and dissertation copies are in typewriter face, while others may be from any type of computer printer.

The quality of this reproduction is dependent upon the quality of the copy submitted. Broken or indistinct print, colored or poor quality illustrations and photographs, print bleedthrough, substandard margins, and improper alignment can adversely affect reproduction.

In the unlikely event that the author did not send UMI a complete manuscript and there are missing pages, these will be noted. Also, if unauthorized copyright material had to be removed, a note will indicate the deletion.

Oversize materials (e.g., maps, drawings, charts) are reproduced by sectioning the original, beginning at the upper left-hand corner and continuing from left to right in equal sections with small overlaps.

Photographs included in the original manuscript have been reproduced xerographically in this copy. Higher quality 6" x 9" black and white photographic prints are available for any photographs or illustrations appearing in this copy for an additional charge. Contact UMI directly to order.

Bell & Howell Information and Learning
300 North Zeeb Road, Ann Arbor, MI 48106-1346 USA
800-521-0600

Properties

of Magnetization Tunneling in High-Spin Molecules

at Low Temperature

by

Yicheng Zhong

A dissertation submitted to the Graduate Faculty in Physics in partial fulfillment of the requirements for the degree of Doctor of Philosophy, The City University of New York.

2001

Bell & Howell Information and Learning Company
300 North Zeeb Road
P.O. Box 1346
Ann Arbor, MI 48106-1346

This manuscript has been read and accepted for the Graduate Faculty in Physics in satisfaction of the dissertation requirement for the degree of Doctor of Philosophy.

December 5, 2000
Date

Myriam P. Sarachik
Chair of Examining Committee

12/12/00
Date

Executive Officer

Prof. Joseph Birman

Prof. Fred Cadieu

Prof. Eugene Chudnovsky

Prof. Frederick Smith

Supervisory Committee

THE CITY UNIVERSITY OF NEW YORK

ABSTRACT

Properties
of Magnetization Tunneling in High-Spin Molecules
at Low Temperature

by

Yicheng Zhong

Thesis Advisor: Dist. Professor Myriam P. Sarachik

Based upon several interesting experiments, this thesis aims to address some deeper properties of Quantum Tunneling of Magnetization in Mn_{12}-acetate, a high-spin molecular maget at low temperature. After a brief introduction (Chapter 1), I will show data obtained from Inelastic Neutron Scattering experiments in Mn_{12} revealing the presence of higher order uniaxial anisotropy (Chapter 2), a term central to the discussion of the results presented later. Chapter 3 will deal with a study of the magnetic relaxation of single crystals of Mn_{12} in the regime of thermally assisted tunneling; complex features were found within each resonance which are not fully understood at this time. In Chapter 4 I will describe a sensitive Hall bar technique for measuring the magnetization of micron-size samples at very low temperature. I will present experimental data of hysteresis obtained at temperatures down to 0.4 K in Mn_{12}, and then interpret the data in light of the higher-order anisotropy and the theory of the first-order transition in Mn_{12}. A separate study of the effect of a transverse magnetic field on the lineshape of the $N = 0$ resonance in Mn_{12} will be presented in Chapter 5. It will help further identify the unsolved key issues related to the tunneling mechanism in Mn_{12}. I will conclude my dissertation with a summary and suggestions for future studies in Chapter 6.

DEDICATION

To my dear wife and parents

ACKNOWLEDGEMENTS

My heartfelt thanks go to many people who gave me vital support during my thesis research. With them, this fascinating five years of Ph.D. study constitute my most enjoyable memory.

Professor Myriam Sarachik, my thesis mentor, is a rare experimental physicist with whom I enjoyed tremendous opportunity of academic growth. Her superb taste of value in physics, sharp insight of essentiality within complexity, transparent explanation of brainstorm during discussion and enthusiastic pursuit of answer via experimental revelation orchestrate the whole research activities of our group. I am very fortunate to have her guidance and support in all phases of this research work. Her inspiring optimism and detailed suggestions always came to rescue at times when I most need them.

I am also deeply indebted to Dr. Jonathan Friedman, a former member in Sarachik group whose influence on my research cannot be more emphasized. He trained me wholeheartedly on magnetization measurements techniques when I first joined the group and remained my most trustworthy and respected friend of help, comment, and sometimes, criticism in physics. He is responsible for suggesting the experiment leading to findings of rich structures within Mn_{12}'s tunneling resonances (see Chapter 3). I enjoyed working closely with him on neutron scattering experiments at Los Alamos and on several other important occasions.

I am grateful to Professor Eugene Chudnovsky, a central theorist in macroscopic quantum tunneling who kindly undertook the task of instructing me on the fundamentals of magnetism theory in a special course. As our "theoretical wisdom", he tirelessly educated us on most recent theoretical developments and generously provided his comments on my work, always at ease conveying key theoretical messages to experimental ears without elaborate math.

I am thankful to Dr. Robert Robinson, a former senior research scientist at Los Alamos Neutron Science Center with whom I enjoyed a fruitful and memorable collaboration. It's a great pleasure working with Rob, and many other colleagues at Los Alamos and Argonne. Among them are Dr. Heinz Nakotte, Dr. Frans Trouw, Timothy Kelly, Andrew Christianson with whom I feel strongly that doing physics is like joining a club: the more you input, the more fun you have.

As our collaborator in Chemistry, Professor David Hendrickson provided us with all the nice Mn_{12} samples. I'd like to thank Dr. Sheila Aubin, Dr. Daniel Ruiz, and Jae Yoo in his group for their professional work.

Professor Andrew Kent at New York University gave me the opportunity to experiment low temperature single crystal magnetization measurement on his micron-sized Hall bars through its success in January 1999. Louisa Bokacheva, a Ph.D. student in Kent's group, provided me with substantial help during this process.

I am grateful to Dr. Eli Zeldov and his student Yossi Paltiel for their high-quality Hall sensors and very helpful suggestions on effective usage of them in our He_3 cryostat.

I owe a lot to Kevin Mertes, a fellow Ph.D. student in Sarachik group. Kevin's expertise in electronics and computer technology forms a valuable asset to all of us in the group. Dr. Snezana Bogdanovich, a former student of the group, trained me on low temperature techniques in general by giving me the opportunity to help on her very interesting stress-tuned Metal Insulator Transition (MIT) experiments. I would also like to thank Dr.s Sergey Vitkalov, Dmitri Simonian and Sergey Kravchenko for their constant help and interest in my research work. Their probing questions helped me understand my physics better.

Professor Joseph Birman have always expressed interest in my field and my work. I am very much grateful for his substantial help, both scientific and personal, during the years I spent at City College.

Professors Frederick Smith, Marilyn Gunner and Herman Cummins generously allowed me to use their lab equipments and were "happy to see science happen" through that (as by Professor Gunner).

I also wish to thank the memebers of my thesis committee , including Professor Fred Cadieu other than those mentioned above, for their interest in this field and for reading this manuscipt.

I am grateful to the U.S. National Science Foundation who supported my thesis research during these years.

Lastly, I would like to thank my wife, Wenjie for her perpetual support in my research, especially (and most memorably) for the wonderful late-night food she sent in for me in those days when I worked into early mornings at NYU. I am also grateful to my parents whose encouragement and advice always make me more confident in face of difficulties.

Contents

List of Figures

List of Tables

Chapter 1

Introduction

Quantum tunneling of magnetization (QTM) has been an active area of extensive theoretical and experimental research for more than a decade. The strong interest in macroscopic magnetization tunneling, in which a large magnetic moment ($S \gg 1$) tunnels quantum-mechanically between its classically stable magnetic configurations, stems from its importance as a fundamental problem in physics, and the potential for applications. From a fundamental point of view, physicists are fascinated by observations of quantum mechanical processes that are manifested on a macroscopic scale, such as superconductivity, superfluidity and the laser. Leggett and his co-workers pointed out in the 1980s that a macroscopic object with many microscopic degrees of freedom could behave quantum mechanically provided it is sufficiently decoupled from its environment [1, 2, 3]. In magnetism, a single-domain particle consisting of a large number of atomic spins coupled strongly at low temperatures has been considered a candidate for the study of behavior that is borderline between classical and quantum physics [4]. From the point of view of applications, the study of magnetic tunneling is important for understanding the ultimate (quantum) limitations on the size of an individual magnetic memory unit, and it may also hold promise for quantum computation [5].

Earlier investigations of magnetization tunneling in nanomagnets were complicated by difficulties in producing systems of small and identical magnetic particles. Size, shape and orientation distributions usually result in an averaged effect which makes rigorous comparison with theory difficult [6]. Molecular chemistry suggested a different approach to grow well defined magnetic clusters of metal ions which are nominally identical and regularly arranged on a crystal lattice. To date, the best known systems of this kind are Mn_{12}-acetate [7] ($[Mn_{12}O_{12}(CH_3COO)_{16}(H_2O)_4]\cdot 2CH_3COOH\cdot 4H_2O$), hereafter referred to simply as Mn_{12}, and ($[Fe_8O_2(OH)_{12}(tacn)_6]^{8+}$), generally referred to as Fe_8 [8]. These monodispersed systems provide a unique laboratory for the study of QTM, since they can be well characterized, leaving no room for arbitrary free parameters.

An important milestone in the study of QTM was achieved when Friedman *et al.* found compelling evidence of spin tunneling in Mn_{12}. They discovered a series of nearly equally spaced steps in the hysteresis loops of an oriented powder sample below the blocking temperature of about 3 K [10], which they attributed to "thermally assisted tunneling" of the magnetization [11]. These results were soon confirmed in studies of single crystals of Mn_{12} [12]. Similar steps have subsequently been found in the hysteresis of several other materials including Fe_8 [13].

In this dissertation, I will present experimental data on Mn_{12} which reveal richer features of this fascinating system. Most of the results can be explained in terms of a higher order uniaxial anisotropy term in the $S = 10$ spin Hamiltonian of Mn_{12} which produces a slight difference in magnetic fields for different pairs of levels coming into resonance. A detailed investigation of the dominant tunneling path at various temperatures shows an abrupt transition between the regimes of thermally assisted

tunneling and ground state tunneling, as suggested by a recent theory of Chudnovsky and Garanin [14].

In the remainder of this chapter, I will first provide relevant background information on Mn_{12}, focussing on recent work in characterization of the system; I will then review the concept of thermally assisted magnetization tunneling which will serve as a basis of discussion of work presented later in this thesis. I will conclude this chapter by examining an interesting problem studied theoretically by Chudnovsky and Garanin concerning the abrupt or continuous nature of the transition of a system of spins from thermally assisted to pure quantum tunneling.

The other parts of the manuscript are organized as follows: in Chapter 2 I will show data obtained from Inelastic Neutron Scattering experiments in Mn_{12}. These studies revealed the presence of higher order uniaxial anisotropy in Mn_{12}, a term which is central to the discussion of our experimental results presented in the subsequent two chapters. Chapter 3 will deal with a study of the magnetic relaxation of single crystals of Mn_{12} in the regime of thermally assisted tunneling (above 1.8 K); complex features were found within each resonance which are not fully understood at this time. In Chapter 4 I will describe a sensitive Hall bar technique for measuring the magnetization of micron-size samples at very low temperature. Following a discussion of the technical details of these measurements, I will present experimental data of hysteresis obtained at temperatures down to 0.4 K in Mn_{12}, and then interpret the data in light of the higher-order anisotropy and the theory of the first-order transition in Mn_{12}. A separate study of the effect of a transverse magnetic field on the lineshape of the $N = 0$ resonance in Mn_{12} will be presented in Chapter 5. It will help further identify the unsolved key issues related to the tunneling mechanism in

Mn_{12} (most noticeably, the puzzling role of hyperfine field in the tunneling process of this material). I will conclude my dissertation with a summary and suggestions for future studies in Chapter 6.

1.1 Background on Mn_{12}-acetate

Mn_{12} had drawn much attention even before the breakthrough made by Friedman *et al.* [10]. First synthesized by Lis in 1980 [7], this material consists of Avogadro's number of weakly interacting, chemically identical Mn_{12} molecules residing on a body-centered tetragonal latice. As shown in Fig. 1.1, each molecule contains four Mn^{4+} ($S = 3/2$) ions on a central tetrahedron surrounded by eight Mn^{3+} ($S = 2$) ions forming an outer ring. Superexchange coupling through oxygen bridges between Mn ions results in an $S = 10$ ground state at low temperatures [15]. A strong magnetocrystalline anisotropy splits the ground state into 21 sublevels with the uniaxial anisotropy axis coinciding with the crystal's c-axis [16]. Dipole-dipole interactions between neighboring molecules are small because nonmagnetic components surrounding each magnetic core keeps magnetic clusters well separated; the Curie-Weiss temperature for this system has been measured to be small (between -50 and $+70$ mK) [17, 18]. The spin 10 lies in a magnetic regime that marks the boundary between atomic and macroscopic scales, and thus represents a very interesting object for study.

Strong evidence for resonant spin tunneling in Mn_{12} was provided by the experiments of Friedman *et al.* [10] in 1996, with the discovery of a series of steps in the hysteresis loops of Mn_{12}. The system was modeled as a double-well potential, shown

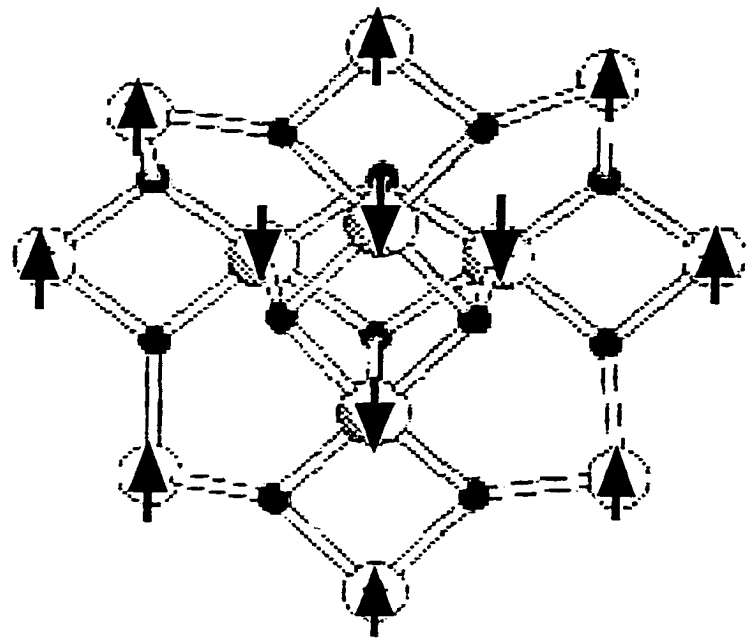

Figure 1.1: **Structure of Magnetic core of Mn_{12} molecule. Four Mn^{4+} ions ($S = 3/2$, pointing downwards) and eight Mn^{3+} ions ($S = 2$, spointing upwards) are strongly coupled through oxygen bridges (small dots) to form a rigid spin $S = 10$ at low temperature.**

in Figure 1.2, with each molecule's $(2S + 1) = 21$ states yielding two degenerate ground states $m = \pm 10$, and a set of doubly degenerate excited states $m = \pm 9, \pm 8$ ...(except for $m = 0$) in zero field. A magnetic field along the easy axis tilts the potential. At specific values of magnetic field, levels in opposite wells come into resonance and spin tunneling occurs across the anisotropy barrier, resulting in a much faster interwell relaxation rate giving rise to steps in the hysteresis loops. To lowest order, Mn_{12} has been described by the simple Hamiltonian [10]:

$$\mathcal{H} = -DS_z^2 - g\mu_B \mathbf{H} \cdot \mathbf{S} \tag{1.1}$$

where the z-axis is chosen along the anisotropy axis. $D \approx 0.6$ K represents the uniaxial anisotropy that breaks the 21-fold degeneracy of Mn_{12}-acetate's spin-10 states and the second term represents the Zeeman energy. With this simple Hamiltonian, pairs of levels on opposite sides of the barrier all cross simultaneously, *i.e.*, their energies coincide[1]. The level(s) from which tunneling proceeds depends on temperature (see the following section on "thermally assisted tunneling").

Many interesting papers appeared after this breakthrough, some based on other experimental techniques, which further established the quantum mechanical nature of the abnormally faster relaxation in Mn_{12}, and which provided additional valuable insights into this problem. Using a sensitive heat capacity measuring device, Fominaya *et al.* [20] and Gomes *et al.* [21] found specific heat anomalies at the magnetic field values that correspond to the crossing of spin up and spin down levels of different magnetic quantum numbers *above* the blocking temperature ($T_B \approx 3$ K) of Mn_{12}. In addition, heat relaxation pulses were observed *below* T_B when the fields were applied antiparallel to the initial magnetization at those field values. All these results were explained in terms of magnetization tunneling between spin states. Using ac magnetic

[1]This point will be revisited in Chapter 2 in which higher order anisotropy terms are considered.

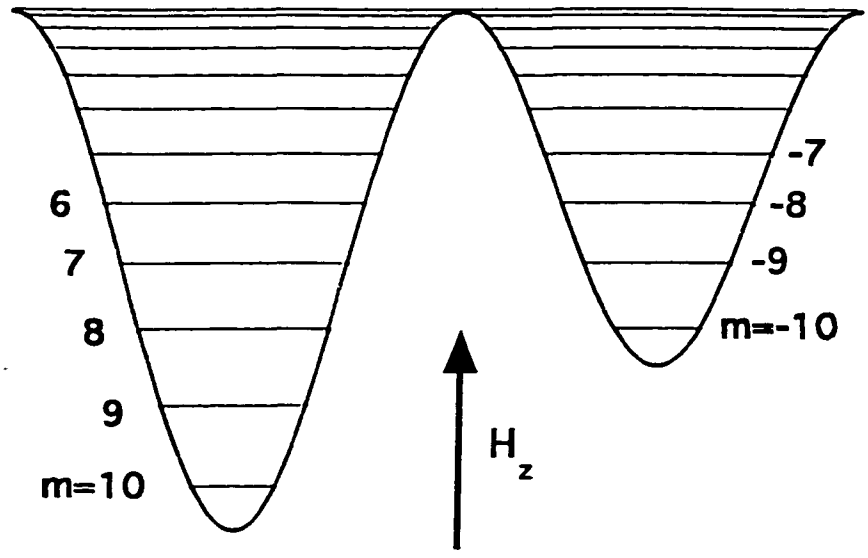

Figure 1.2: **Double-well potential of spin-10 molecules such as Mn_{12}. Different levels correspond to different spin projections along the magnetic anisotropy axis along which a magnetic field is applied.**

susceptibility techniques, Luis *et al.* [22] confirmed that there is field-tuned tunneling between excited magnetic states which are thermally populated. The effect of a transverse magnetic field on tunneling in Mn_{12} was studied by Friedman *et al.* [23] who found that the transverse field does not change the longitudinal field at which tunneling occurs; instead, it significantly increases the relaxation rate, both on and off resonance.

Characterization of Mn_{12} forms another important area in recent developments. Accurate, reliable experimental determinations of the spin Hamiltonian for Mn_{12} provide crucial information for theorists to calculate QTM in this system. Up to fourth-order terms, the spin Hamiltonian for Mn_{12} can be written as,

$$\mathcal{H} = -DS_z^2 - \mu_B \mathbf{H} \cdot \mathbf{g} \cdot \mathbf{S} - AS_z^4 + C(S_+^4 + S_-^4) \tag{1.2}$$

where the first term represents the leading uniaxial anisotropy, the second term represents the Zeeman energy, and the last two terms presents the higher-order uniaxial anisotropy and the lowest-order off-diagonal transverse anisotropy allowed by the tetragonal symmetry in Mn_{12} crystal. Two Electron Paramagnetic Resonance (EPR) measurements performed in Mn_{12} have yielded different sets of values for the coefficients D and A of Eq. 1.2. Barra *et al.* [24] measured high-field EPR spectra at frequencies ranging from 150 to 525 GHz in magnetic fields up to 25 T on a polycrystalline powder sample, and obtained $g_{||} = (1.93 \pm 0.01)$, $g_{\perp} = (1.96 \pm 0.01)$, $D = (0.56 \pm 0.04)$ K and $A = (1.1 \pm 0.1) \times 10^{-3}$ K. Hill *et al.* [25] studied a submillimeter single crystal using high-sensitivity EPR techniques in the frequency range between 35 and 115 GHz; their results imply $D = 0.59$ K and $A = 0.88 \times 10^{-3}$ K [26] with $g_{||}$ ranging from 1.97 to 2.08 and $g_{\perp} = 1.9$. Although the results do not agree numerically, both experiments indicate the presence of a fourth order term $-AS_z^4$ in the spin Hamiltonian of Mn_{12}. As I will show later in this thesis, inelastic neutron

scattering experiments have helped to resolve the numerical inconsistency.

An inelastic neutron scattering study by Hennion *et al.* [27] of partially deuterated Mn_{12} found a well-defined peak around 0.3 THz (1.24 meV) which was attributed to excitations from $m = \pm 10$ to ± 9. The peak broadens on its low energy side as the temperature increases, but these authors were unable to resolve any detailed structure. Very recently, Robinson *et al.* used neutron diffraction experiments to determine more accurately the structure factors in Mn_{12} [28] and then applied this knowledge to obtain the internal magnetic structure of the molecule. Their results confirmed [29] the standard picture of the Mn_{12} spin-10 cluster at low temperatures.

1.2 Thermally-assisted tunneling in Mn_{12}

The experimental fact [10] that the magnetic relaxation rate of Mn_{12} has maxima at fields corresponding to specific level crossings clearly establishes its quantum nature. On the other hand, the fact that the relaxation rate on resonance decreases rapidly as the temperature is reduced indicates that the resonant tunneling is thermally assisted. For the case of zero longitudinal field, Garanin [30] added a symmetry-breaking term due to a transverse magnetic field to the simple Hamiltonian (Eq. 1.1); consistent with the WKB approximation, he showed that the tunneling rate for degenerate pairs of levels is a very strong function of m, with states near the top of the barrier having much faster rates than states near the bottom. To obtain a reasonably fast tunneling rate comparable to the time scale of a typical DC magnetization measurement, only levels near the top of the anisotropy barrier can be responsible for tunneling

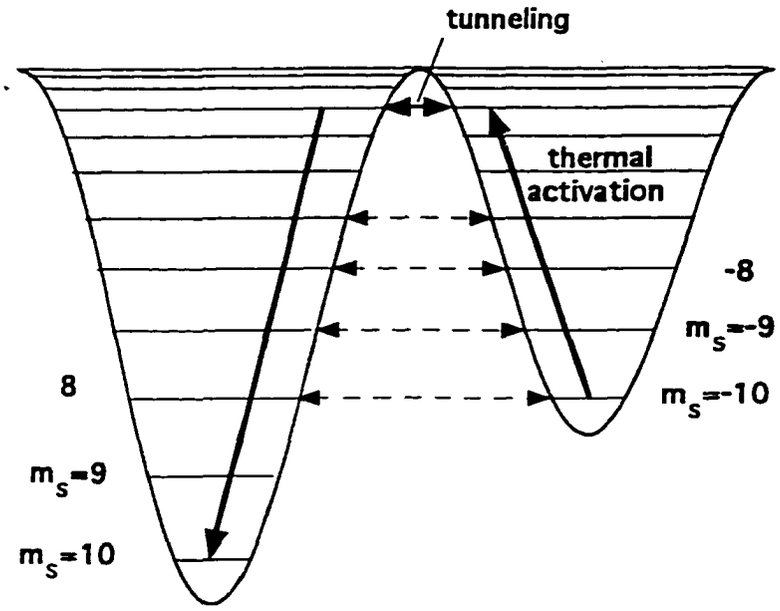

Figure 1.3: **Illustration of "Thermally Assisted Tunneling" in a double well potential. Spins are thermally activated to some level(s) near the top of anisotropy barrier through which tunneling relaxation proceeds at a much faster rate.**

of the molecular magnetic moments in Mn_{12}. Therefore, the QTM in Mn_{12} must be thermally assisted.

First suggested by Novak and Sessoli [11], the "thermally assisted tunneling" model states that magnetization tunneling is dominated by one or a few adjacent thermally populated excited levels. In this picture, spins are thermally activated to some excited state(s) in the metastable well, from which they tunnel across the bar-

rier and then decay to the ground state in the stable well, as illustrated in Fig. 1.3. Two competing factors come into play in this process: one is the thermal population probability which decreases exponentially with excitation energy, $\exp(-E/kT)$; the other is the tunneling probability which increases exponentially with energy E, as the effective barrier height becomes lower and its angular width becomes "thinner". Therefore, a compromise between these two factors must be found which leads to the fact that tunneling occurs only from one or a few adjacent levels near the top of the anisotropy barrier. The level (or group of levels) that dominates the relaxation thus varies strongly with temperature, as has been observed experimentally at temperatures between 1.7 and 3 K [10, 22, 23], a regime in which the model of thermally assisted tunneling can be suitably applied.

Although the model of thermally assisted tunneling successfully addresses the main characteristics of the tunneling process in Mn_{12}, quantitative comparison between experimental data and theoretical calculations requires further knowledge beyond this model. Under what conditions can one observe quantum tunneling of the magnetic moment? What is the mechanism responsible for QTM in Mn_{12}? What is the major symmetry breaking term that drives tunneling? These are all very important questions which need to be addressed. The fact that there is no obvious selection rule in the magnetic hysteresis of Mn_{12} strongly suggests that the presence of a transverse magnetic field is mainly responsible for tunneling. Since no such field was applied externally in the experiments, it has been suggested that the transverse component of an internal field of dipolar or hyperfine origin may be responsible [31, 32]. Hyperfine fields in Mn_{12} have been estimated to be 300–500 Oe [33] while dipolar fields are too weak to drive tunneling compared to hyperfine fields and can therefore be ruled out [34]. Considering the random nature of hyperfine fields, inhomogeneous

broadening of the resonances should be expected. However, a detailed lineshape study by Friedman *et al.* [35] in the neighborhood of the zero-field resonance revealed a Lorentzian lineshape which showed no hint of inhomogeneous hyperfine broadening. The linewidth of the Lorentzian lineshape corresponds to a time scale which is not related to any relevant microscopic time scale known for the system (neither the Arrhenius prefactor nor the precession frequency of spin-10 in the anisotropy field) and raises further questions about the origin of the tunneling mechanism. In Chapter 5, a further complementary study using transverse magnetic field will be discussed.

With the spin Hamiltonian containing higher order anisotropy terms, Fort *et al.* [36] have presented a calculation of the resonance lineshape near zero field using fourth-order transverse anisotropy $C[S_+^4 + S_-^4]$ as the symmetry breaking term. However, the fits to the data become worse at fields farther from $H = 0$ and the authors also noted that half the experimentally observed resonance peaks would be missing if the fourth-order anisotropy were solely responsible for tunneling. Luis *et al.* [37] calculated the joint effect of transverse magnetic field and fourth-order transverse anisotropy to account for QTM in Mn_{12}. However, a straightforward implication of their work would be an alternating change in *amplitude* between odd and even resonances which has not been established experimentally. Very recently, Leuenberger and Loss [38] presented a theory of the magnetization relaxation in Mn_{12} in the high temperature regime ($T \geq 1$ K) based on phonon-assisted spin tunneling induced by quartic magnetic anisotropy and weak transverse magnetic fields. The main features of their fits qualitatively agree with experimental data even though many details are not accounted for (e.g. the fit to data in ref. [35] failed systematically to fit the tail of the Lorentzian lineshape), indicating other complexity in the system which is not accounted for in their calculation.

1.3 Relaxation of the magnetization at lower temperatures

Since the discovery of steps in the hysteresis loops of Mn_{12} in the temperature range 1.7–3K, theory has been challenging experimentalists to perform magnetic measurements at even lower temperatures on these "tunneling nanomagnets" to explore novel physics.

Transitions between two states in a bistable system can occur either due to the classical thermal activation or via quantum tunneling. For Mn_{12}, the observed magnetic relaxation is a combination of these two processes. At high temperature (superparamagnetism) thermal activation dominates the relaxation process and the classical Arrhenius law is observed for the relaxation rate, $\Gamma \sim \exp(-U/T)$, with $U \approx 60K$ being the barrier height [40]; in the low temperature limit the relaxation is (supposed to be) pure ground state tunneling and Γ becomes independent of temperature; thermally assisted tunneling defines a regime intermediate between the above two regimes in which both thermal activation and quantum tunneling are important to the magnetization reversal.

It is well known from early experimental work on Mn_{12} that the boundary between the regimes of thermal over-barrier activation and thermally assisted tunneling is the blocking temperature, $T_B \approx 3$ K, below which hysteretic behaviour starts to set in for Mn_{12} [40, 41]. The other boundary between thermally assisted tunneling and ground state tunneling, however, turns out to be even more interesting. Fascinating physics has been developed related to *this boundary* for a uniaxial spin system like

Mn_{12} which provides us with a surprising example of how pure quantum mechanical tunneling is reached.

Recently Chudnovsky and Garanin [14] found a novel feature in the escape rate of a bistable large spin system described by the Hamiltonian

$$H = -DS_z^2 - H_x S_x. \tag{1.3}$$

In particular, they found that the the escape rate can undergo a transition from the classical to the quantum regime that is sharp (first-order) or smooth (second-order), depending on the strength of the transverse magnetic field. The analogy with phase transitions was first made by Larkin and Ovchinnikov [42] and holds strictly only in the limit of $S \to \infty$. However, as pointed out by Chudnovsky and Garanin, even for a moderate spin like $S = 10$ in Mn_{12} where quantization of spin levels becomes important, the major results regarding the first- and second-order nature of the transition remain valid except for an accuracy of $1/S$ in the transition. This work was later generalized to the case of an arbitrarily directed field [43] and also to a biaxial spin system (like Fe_8) [44].

The temperature dependence of the level from which dominant tunneling happens (labeled by the quantum number m_{TAT}) is illustrated in Figure 1.4, taken from Figure 3 in ref. [32]. Two different scenarios can be clearly seen. At high values of transverse magnetic field h_x (which favors the second-order transition), m_{TAT} can shift continuously with increasing temperature from the bottom to the top of the barrier through each value of m and finally merge with the horizontal line characterizing the Arrhenius regime. In contrast, in lower transverse fields h_x (which favors the first-order transition) large jumps of m_{TAT} can be seen, implying that tunneling from levels in the middle of the barrier are skipped entirely when temperature is raised.

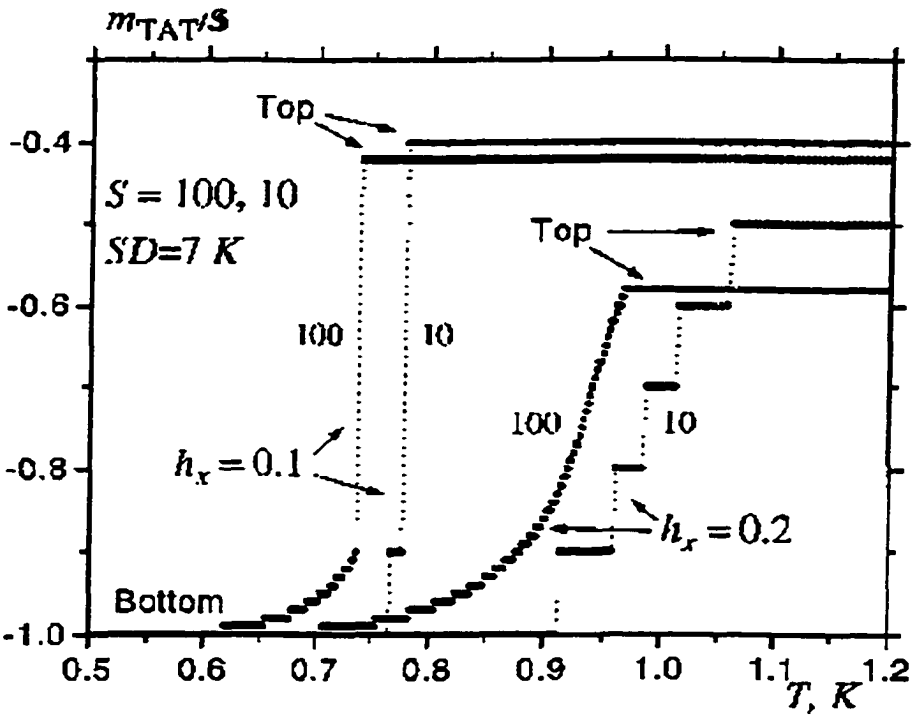

Figure 1.4: **Calculated dominant tunneling level plotted as a function of temperature (from Ref. [32]). At large/small transverse magnetic field, this level changes continuously/abruptly with temperature for both spin-10 and spin-100 systems.**

In this case, there are two maxima, or competing channels of relaxation at the top and near the bottom of the barrier which go from one into the other at the transition temperature. Please note that the same kind of jump is seen for "large" ($S = 100$) as well as moderate ($S = 10$) spins, whether level quantization is important to the problem or not.

Intuitively, smooth (or second-order) classical-quantum transitions of the escape rate are common, whereas abrupt (or first-order) transitions between the two regimes are unexpected. In their original work [14], Chudnovsky and Garanin performed their calculation by mapping the spin problem with the Hamiltonian of Eq. 1.3 onto an equivalent problem of a particle moving in a double-well potential $U(x)$, a method which leads to a more transparent and solid understanding of the problem — Qualitatively, let us study a barrier $U(x)$ with a rather flat top and two steep sides like that plotted in Fig. 1.5. For such a "rectangular" barrier, tunneling through the middle part of the barrier is not favorable since the WKB tunnelling probability is not increased substantially compared to the bottom part whereas the thermal population is much decreased (exponentially). Therefore, thermally assisted tunneling through this part of the potential barrier is suppressed, and thermally assisted tunneling near the top of the barrier competes directly with the ground-state tunneling. A slight change in temperature near the transition point can cause a dramatic switch in tunneling between these two totally different parts of the barrier and lead to a first-order transition.

The estimated crossover temperatures of about 1 K for Mn_{12} and about 0.8 K for Fe_8 are both substantially lower than the lowest temperature achievable (1.6–

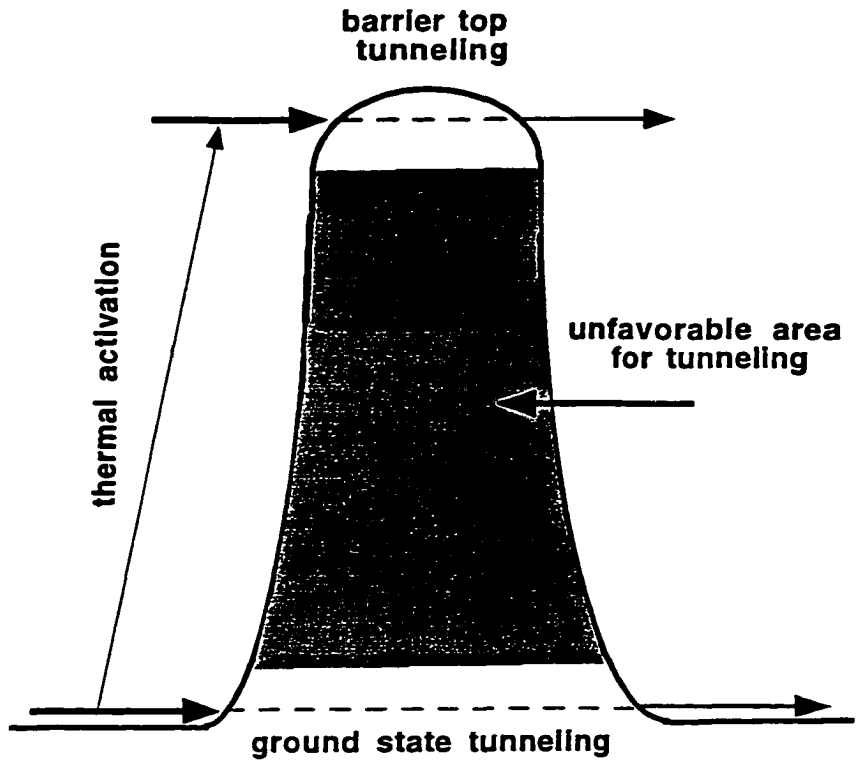

Figure 1.5: **Illustration of abrupt transition between tunneling paths through a "rectangular barrier". An intuitive way to understand the abrupt feature of this transition is to think of tunneling through a nearby rectangular barrier. At high temperature, tunneling happens at the top of the barrier. As the temperature is lowered, the ground tunneling channel immediately starts to compete with the top channel since the much larger spin population is more favorable to tunneling.**

1.7 K) with a commercial (Qantum Design)[2] SQUID magnetometer. A five-fold reduction in temperature can be obtained in a ^{3}He cryostat (which typically reaches temperatures of 0.3 K), and an additional factor of five is available in our dilution refrigerator (60 mK). For Mn_{12} one expects to find interesting, and perhaps dramatic, experimental outcomes if high-sensitivity magnetometry can be performed over such a broad range of temperature (see Chapter 4 for such a technical solution which enables these studies).

The relaxation of the magnetization of Mn_{12} has been explored by Perenboom *et al.* [46] with a cantilever magnetometer to temperatures below 60 mK. Contrary to expectations [31], no steps with indices higher than 11 were observed in the hysteretic magnetization. The long time tail ($t > 2000$ s) of the magnetic relaxation was found to be logarithmic below 1 K, quite different from the exponential decay found in relaxation measurements on the same time scale at high temperatures.

In the coming chapters, I will present our experimental data for the magnetic relaxaton of Mn_{12} at temperatures below 1 K, and provide an interpretation in light of the first-order quantum-classical transition theory discussed above. I will also present results of our inelastic neutron scattering experiments and high temperature relaxation measurements, both of which show the existence of the higher order uniaxial anisotropy in Mn_{12} necessary to explain the "shift" in resonant magnetic fields at lower temperatures.

[2]in contrast to the micro-SQUID magnetometer developed by Wernsdorfer *et al.* [45]

Chapter 2

Inelastic Neutron Scattering Study of Mn_{12}-acetate

Neutron scattering constitutes one of the valuable tools for studying the properties of materials. In particular, inelastic neutron scattering (INS) can be used to probe the energy levels of high-spin molecules. After discussing the advantages of applying neutron scattering to the study of molecular magnets, I will briefly describe the relevant features of QENS at Argonne National Laboratory — the neutron spectrometer on which we performed the INS study in Mn_{12} and acquired high quality data. I will then present experimental data from these studies and end this chapter with a detailed discussion on the crucial information INS reveals concerning the energy spectrum of Mn_{12} and its impact on the study of Quantum Tunneling of Magnetization in this system.

2.1 Background on neutron scattering

Thermal neutron scattering has substantial advantages in the study of high-spin molecular magnets over other spectroscopic methods such as X-ray scattering and Electron Paramagnetic Resonance (EPR) due to the following intrinsic properties of neutrons [52]:

The fact that the neutron is uncharged means that it can not only penetrate deeply into the target, but also that it comes close to the nuclei since there is no Coulomb barrier to overcome. Therefore neutrons are scattered by nuclear forces, not by the Coulomb forces of the electrons, as in X-ray scattering.

The de Broglie wavelength of thermal neutrons is comparable to atomic spacings and the kinetic energy of neutrons is comparable to the energy of phonons in solids, making it an ideal probe for the structure analysis of high-spin molecules in a crystalline form such as Mn_{12}.

More importantly, the magnetic moment of the neutron enables it to interact with the unpaired electrons in magnetic molecules. Elastic scattering from this interaction gives information on the arrangement of electron spins and the density distribution of unpaired electrons in molecular magnets. Inelastic magnetic scattering yields the energy of magnetic excitations, providing crucial information about the energy-level spectrum of molecular magnets.

Finally, the energy of thermal neutrons is of the same order as that of many excitations in high-spin molecular magnets. The creation or annihilation of an excitation

is aided by an inelastically scattered neutron and the percentage change in the energy of the neutron is a large fraction of its initial (or final) energy, making accurate measurement of the energies of these excitations possible. For example, the energy resolution is at 100 μeV (1.2 K) for the fixed final neutron energy of 3.6 meV (42 K) on the QENS spectrometer. For comparison, one of the major excitations in Mn_{12} molecules is estimated at about 12 K.

Unlike thermal neutron energies, typical X-ray energies are several keV, making X-ray spectroscopy an unsuitable tool to probe the very small energy level spacings in magnetic molecules due to difficulty in energy resolution. Another spectrosopic method, Electron Paramagnetic Resonance has been used widely in the characterization of high-spin molecules [24, 25]. However, EPR measurements are normally done in a magnetic field and the g values, generally unknown, are treated as (additional) fitting parameters. In contrast, Inelastic Neutron Scattering experiments are normally performed in the absence of external magnetic field, and yield a more direct and accurate determination of the energy spectrum of the molecules.

2.2 Inelastic neutron scattering spectrometer — QENS

Our first Inelastic Neutron Scattering experiment on Mn_{12} was done on PHAROS, the Inelastic Neutron Scattering spectrometer at the Los Alamos Neutron Science Center. A 1.24 meV peak was observed at the lowest temperature of 1.6 K. However,

the energy resolution of PHAROS (0.4 meV at fixed initial neutron energy of 12 meV) didn't allow a detailed study to resolve other low energy magnetic excitations within the $S = 10$ manifold of Mn_{12}. Consequently, QENS was proposed as a more suitable spectrometer for investigating the low energy excitations in Mn_{12}.

The Quasielastic Neutron Scattering Spectrometer (QENS) at the Intense Pulsed Neutron Source (IPNS) at Argonne National Laboratory is an inverse geometry crystal analyzer spectrometer that provides full coverage of both quasielastic and inelastic neutron scattering simultaneously from a single sample [53]. Fast neutrons are produced from spallation and fission reactions in a depleted uranium target bombarded by 450 MeV protons in 80 ns-wide pulses. The fast neutrons are then moderated by a liquid methane moderator at 100 K. The low temperature moderator increases the population of neutrons below 20 meV. Therefore, QENS is mainly used as a low energy transfer spectrometer, excellent for the study of low energy (below 20 meV) excitations in high spin molecules like Mn_{12}. The energy resolution of QENS is about 100 μeV FWHM at fixed final neutron energy of 3.63 meV.

The plan view of the spectrometer is shown in Figure 2.1. The basic principle of the inverse geometry spectrometer is that a broad energy bandwidth of neutrons are incident on the sample and those neutrons which scatter with a select energy are Bragg reflected by the analyzer crystals (graphite on QENS) into the detectors. The final neutron wavelength, λ_f, is given by the Bragg scattering condition, $\lambda_f = 2d\sin\theta_c$, and yields an expression for the scattered neutron energy:

$$E_f = \frac{h^2}{8md^2\sin^2\theta_c}. \tag{2.1}$$

For QENS, this fixed *final* neutron energy is set at 3.63 meV. The incident neutron energy is measured by the detected time-of-flight between the monitor and detector.

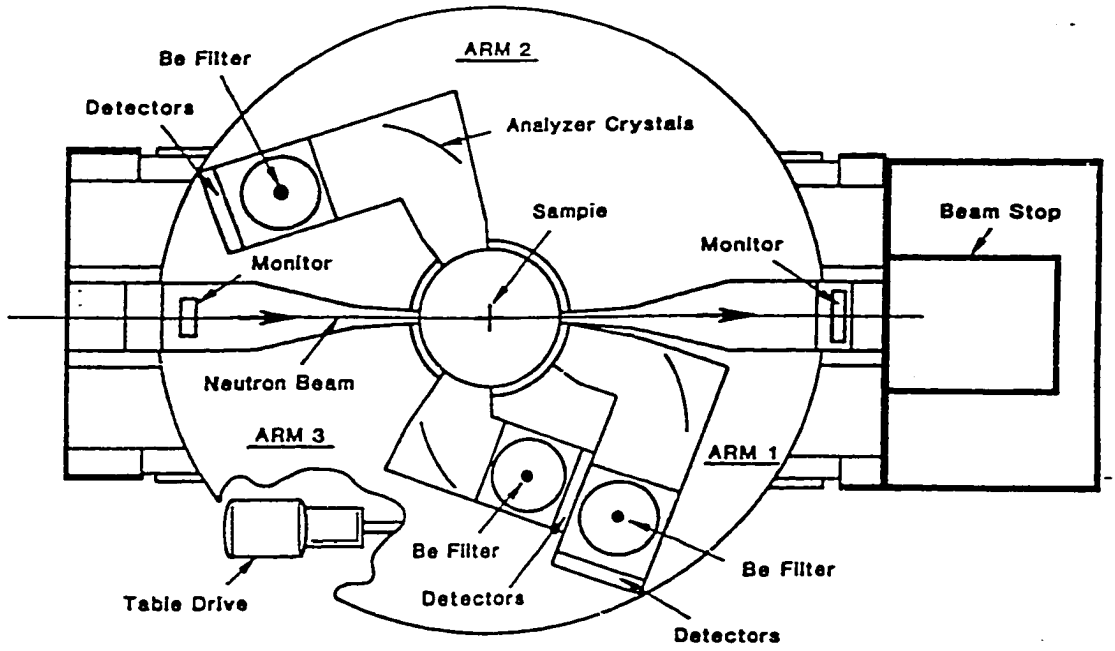

Figure 2.1: **Diagram of Quasi-elastic Neutron Scattering (QENS) spectrometer at Argonne National Laboratory (from Ref. [53]).**

The energy transfer $E = E_f - E_i$ between an individual neutron and the sample can therefore be accurately obtained. If an individual neutron hits a detector oriented at (θ, ϕ), the number of counts n for such an event with parameters (θ, ϕ, E) will be increased by one.

In a real experiment, a time focused neutron beam hits the sample with a high frequency of 30 Hz and the counting numbers $n(\theta, \phi, E)$ soon becomes the statistical average. Important information can be obtained by analyzing the large array $n(\theta, \phi, E)$.

By integrating over all the scattering angles θ and ϕ available in the experiment, the number of counts $n(E)$ contains all the scattering events in which a neutron changes its energy by E. If there is a peak at energy E_0 for curve $n = n(E)$, it means there is an intrinsic excitation with characteristic energy E in the sample.

On QENS, all the scattering experiments are performed in zero magnetic field. Therefore, the double well potential of Mn_{12} mentioned in Chapter 1 is symmetric in these experiments.

2.3 Experiments and results

A 14-gram deuterated Mn_{12} powder sample was prepared by Prof. David Hendrickson's group according to the published procedure [7] for the inelastic neutron scattering experiments. The proton in Mn_{12} has a very large neutron scattering cross section (at 82.03 barn of "Total Bound Scattering Cross Section") so it is replaced chemically by deuterium (at 7.64 barn TBSCS) in order to reduce background scat-

tering. The powder sample was wrapped in an aluminum foil which is"transparent" to thermal neutrons (Aluminum has a very small TBSCS of 1.50 barn) and placed in the center of the sample chamber where the incoming neutron beam and all the scattering paths to detectors join together. A small portion of the powder sample (several mg) was later set in an epoxy at room temperature in a 5.5 T magnetic field for 8 hours. Hysteresis sweeps were then performed to characterize the sample — steps were found for the deuterated sample at the same quantized magnetic fields as published [10].

Data taken at temperatures of 1.4 K, 10 K, 17 K, and 30K are shown in Figure 2.2 where the neutron scattered intensity is plotted as a function of neutron energy transfer E. The large maximum centered about zero energy is due to elastic scattering. At 1.4 K, a single sharp peak is observed at 1.24 meV; this is attributed to excitations from spin states $m = \pm 10$ to $m = \pm 9$ (see diagram of excitations within double well potential of $S = 10$ manifold, Figure 2.3).

Note that at 1.4 K, the overwhelming majority of spins are in the ground states $m = \pm 10$. So this is the only excitation possible at this temperature. As the temperature is raised and some of the spins are thermally activated to higher energy states, new peaks develop on the low energy side of the 1.24 meV peak; we attribute these to transitions from $m = \pm 9$ to ± 8, ± 8 to ± 7, etc. Transitions such as those between $m = \pm 9$ and ± 7 are forbidden by neutron scattering selection rules, $\Delta S = 0, \pm 1, \Delta m = 0, \pm 1$. Due to the increased population of higher energy levels at higher temperature, peaks also appear that are symmetrically placed with respect to $E = 0$ on the neutron energy-gain side. In these cases, neutrons gain quantized energy from the Mn_{12} system when there is enough excited state population. No

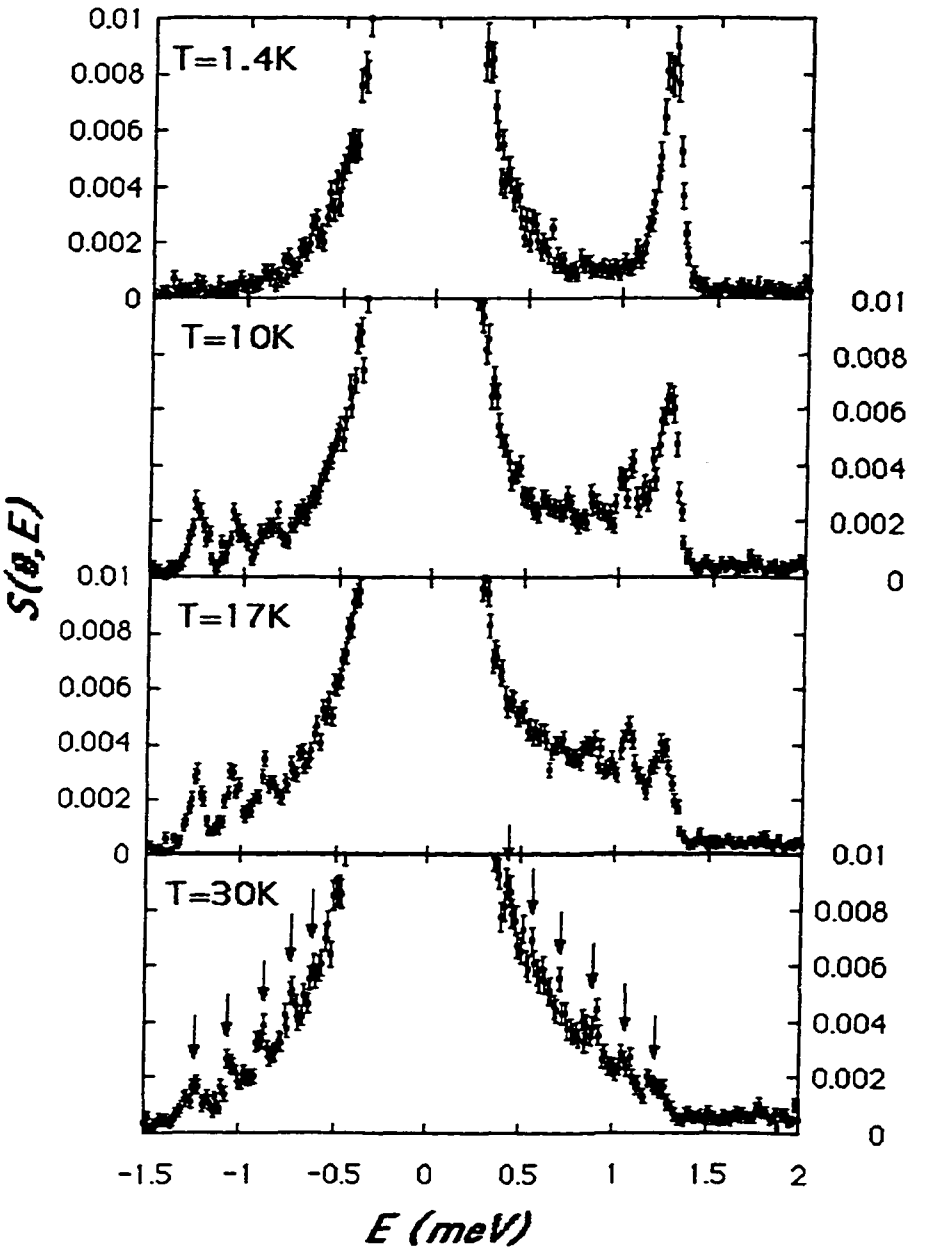

Figure 2.2: **Neutron scattered intensity vs energy at temperatures of 1.4, 10, 17, and 30 K. The spectra shown in this figure were obtained at different scattering angles. The arrows denote the positions of peaks deduced from data taken at all temperatures and scattering angles.**

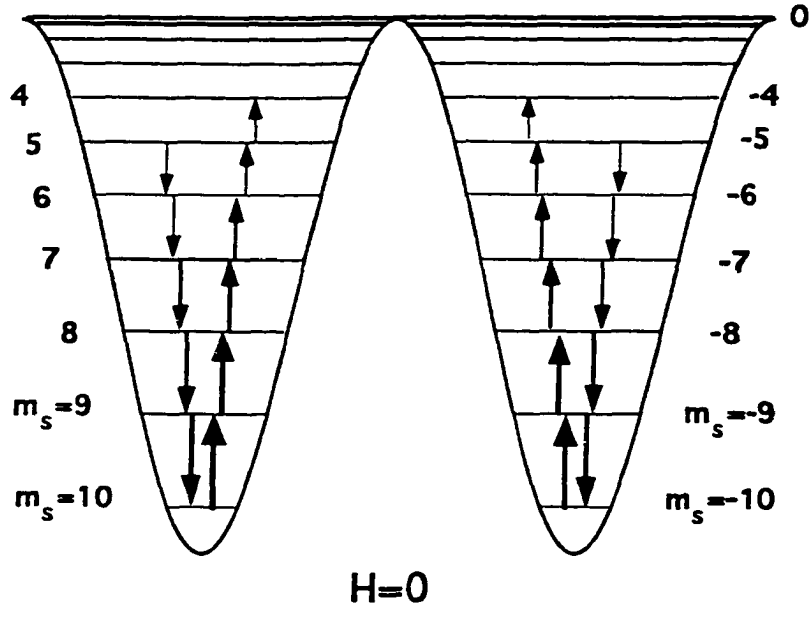

Figure 2.3: **Diagram of excitations within the double well potential. Due to neutron scattering selection rules, only excitations between states of magnetic quantum numbers that differ by one are plotted. The inelastic neutron scattering peaks in Figure 2.2 are directly related to these excitations.**

maxima appear above 1.24 meV up to $\approx$ 3 meV, where further excitations occur that are possibly associated with transitions between different spin manifolds [27]; this further confirms that the peak at 1.24 meV corresponds to transitions between the ground and first excited state of the spin-10 manifold. The maxima are labelled by the index m, which denotes the level from which each excitation occurs; thus, the 1.24 meV peak is labeled 10, the adjacent peak, 9, and so on. As shown below, the positions of these peaks contain key information regarding the spin Hamiltonian of Mn_{12}.

Rewriting the spin Hamiltonian of Mn_{12} here,

$$\mathcal{H} = -DS_z^2 - \mu_B \mathbf{B} \cdot \mathbf{g} \cdot \mathbf{S} - AS_z^4 + C(S_+^4 + S_-^4) \tag{2.2}$$

the following data analysis is applied. Since there is no externally applied magnetic field in our experiments, and the Zeeman energy due to the internal magnetic field of Mn_{12} (estimated to be several hundred Oe [33]) is at least two orders of magnitude smaller than the anisotropy energy, the term $-\mu_B \mathbf{B} \cdot \mathbf{g} \cdot \mathbf{S}$ can be safely neglected. Furthermore, the fourth-order transverse anisotropy term $C(S_+^4 + S_-^4)$ has little effect on the Eigen-energies of the states with large $|m|$ (e.g. for $m = \pm 6$, the perturbation on energy is on the order of $D(\frac{C}{D})^3 \approx 10^{-12} \sim 10^{-11} D$). Therefore, the energy of the states probed in our experiments near the bottom of the anisotropy wells can be approximated by $E_m = -Dm^2 - Am^4$, and the energy of excitation from levels $\pm m$ to $\pm(m-1)$ will be

$$\Delta E_m = E_{m-1} - E_m = D(2m-1) + A[m^4 - (m-1)^4]. \tag{2.3}$$

In Figure 2.4, six excitation energies are plotted as a function of the index m. The deviation from linear dependence clearly indicates the importance of including a

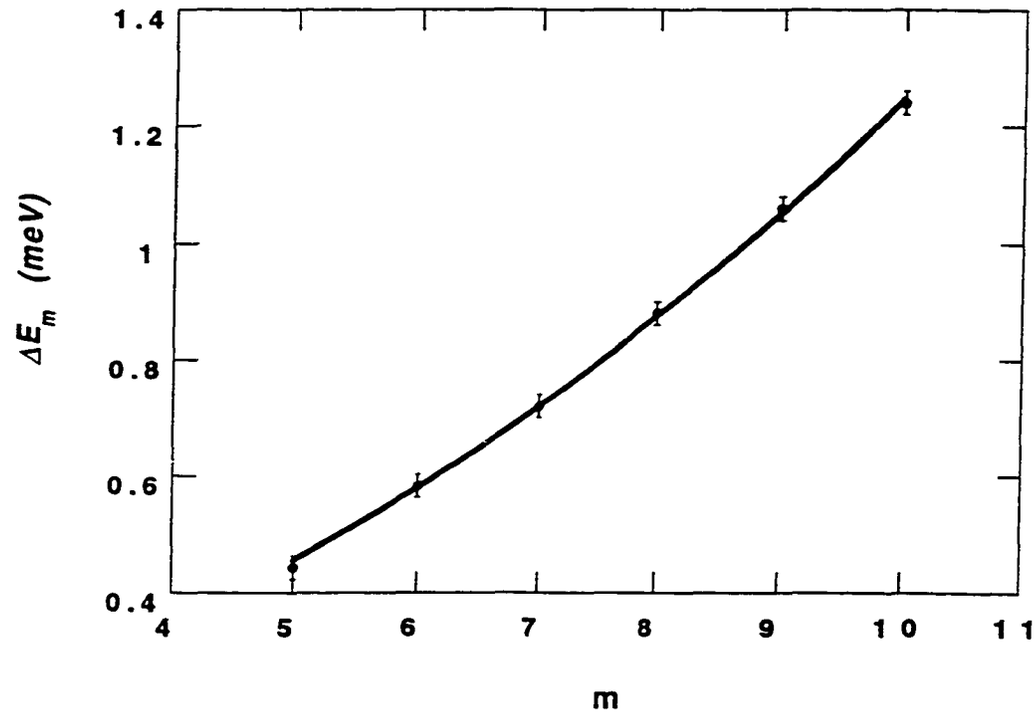

Figure 2.4: **Energies of the peaks of Fig. 2.2 plotted as a function of index m. Index m denotes the initial states for energy loss and final states for energy gain. A two parameter fit to the data yields accurate values for the paramters A and D in the spin Hamiltonian.**

diagonal fourth-order term. A two-parameter fit to Equation 2.3 gives $D = (4.67 \pm 0.18) \times 10^{-2}$ meV=(0.54±0.02) K and $A = (1.04 \pm 0.10) \times 10^{-4}$ meV=(1.2±0.1)$\times 10^{-3}$ K. These values are very close to the EPR results obtained by Barra *et al.*: $D = (0.56 \pm 0.04)$ K, $A = (1.1 \pm 0.1) \times 10^{-3}$ K, and in disagreement with the results of Hill *et al.* [25]. Note that Inelastic Neutron Scattering experiments require no assumption about the Landé factor g, and therefore yield more direct and accurate values of A and D. Our neutron scattering data thus allowed identification of the correct EPR result.

The higher energy part of our data is summarized in Figure 2.5. Hennion *et al.* [27] found similar results in an early study. These excitations are related to excitations from the $S = 10$ spin manifold of Mn_{12} to other spin states (for example $S = 9$, $m = \pm 9$) since it requires much higher energy to break one or several of the superexchange coupled Mn ions within the cluster. As a comparison, the energy scale of the low energy excitations ($E < 1.24$ meV) within the $S = 10$ manifold analyzed above are determined by the magnetic anisotropy, or spin-orbit coupling within the molecule. Several theoretical calculations [54, 55] have been made in order to understand these higher energy excitations. Interpretation of the higher energy spectral features nevertheless remains an open question.

2.4 Discussion

For the values of D and A obtained, the full height of the anisotropy barrier for Mn_{12} (defined as the energy difference between $m = 0$ and $m = 10$) is calculated to be (66 ± 3) K. The ratio $|Am^4/Dm^2| \approx 0.2$ for $m = 10$. The term $(-AS_z^4)$ therefore constitutes a substantial correction to the energy levels near the bottom of

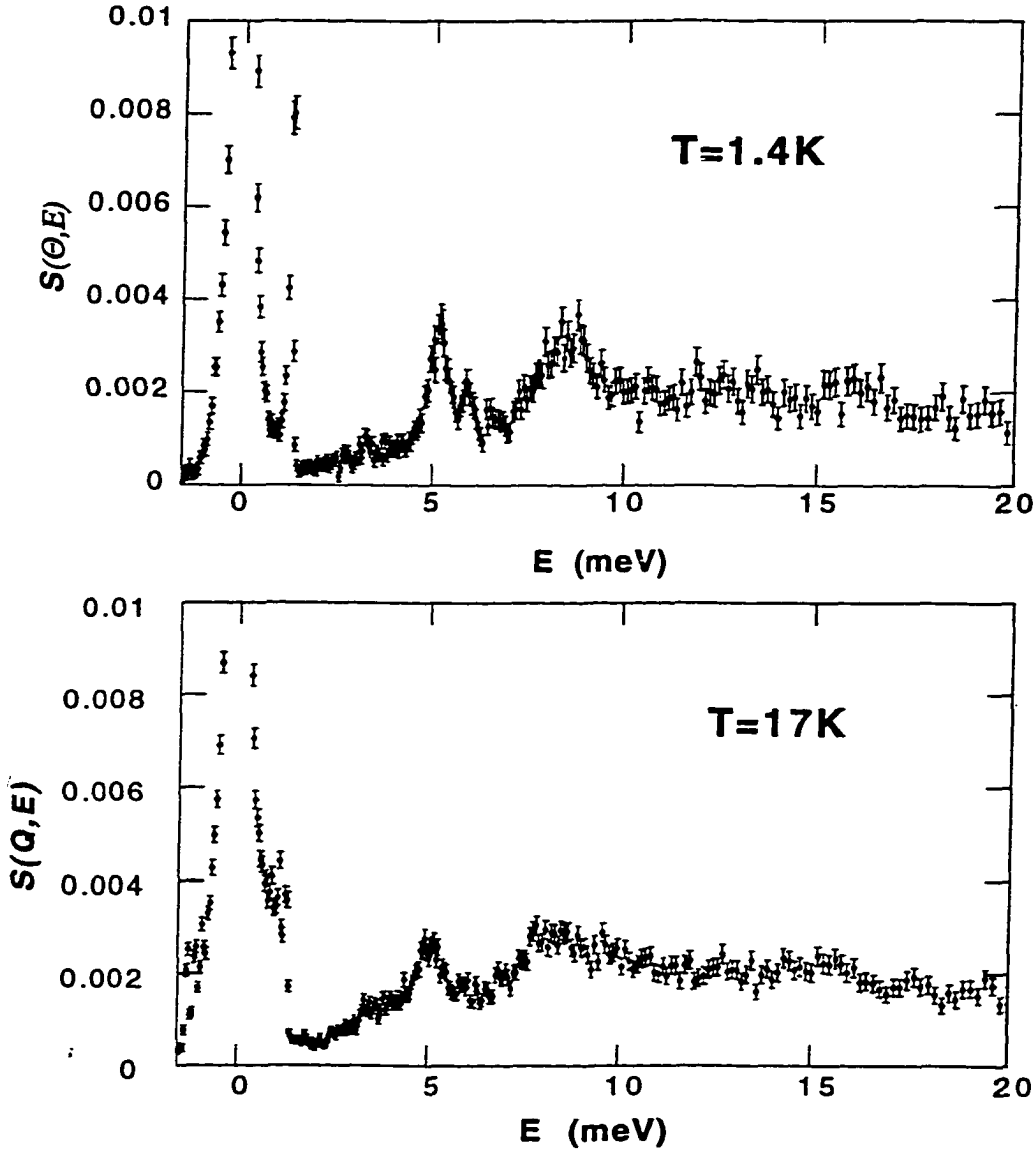

Figure 2.5: **Higher energy part of the neutron scattering scpectra at two temperatures of 1.4 K and 17 K. The sharp peaks above 3 meV are related to excitations between $S = 10$ and other spin manifolds.**

the anisotropy wells. Since A and D have the same sign, the level spacings near the bottom of the wells are relatively sparser, and the distribution of levels near the top of the barrier denser.

Although a higher-order term such as $(-AS_z^4)$ in the spin Hamiltonian of Mn_{12} is generally regarded as a detail, it turns out that the consequences of this term far exceeds that of a trivial "correction". It is *essential* to the study of Quantum Tunneling of Magnetization in Mn_{12}, as will be shown below as well as in experiments described in the next two chapters.

Due to the presence of such a sizable fourth-order term, the energy levels do not come into resonance simutaneously for a given field applied along the anisotropy axis. From the spin Hamiltonian of Mn_{12} (Eq. 2.2), two levels with different quantum numbers m and m' come into resonance when $E_m = E_{m'}$, or at a longitudinal magnetic field H_z given by

$$E_m = -Dm^2 - Am^4 - g_z\mu_B H_z m. \tag{2.4}$$

Combining terms containing H_z, one obtains

$$H_z = NH_0[1 + \frac{A}{D}(m^2 + m'^2)] \tag{2.5}$$

where $H_0 = D/g_z\mu$ and $N = \mid m + m' \mid$. $H_0 = D/g\mu_B$ is defined as the "field quantum" for this system; the N's are the "step numbers" first found experimentally by hysteresis studies [10]. In the absence of the higher order anisotropy $(-AS_z^4)$, levels come into resonance *simultaneously*; *i.e.* if levels m and m' are in resonance, so are levels $(m-1)$ and $(m'+1)$, and so on. However, due to the presence of the higher-order contribution, the term $\frac{A}{D}(m^2 + m'^2)$ causes pairs of levels m and m' to come into resonance at magnetic fields which are not simply determined by the sum of m and m', *i.e.* they do not come into resonance simultaneously. Rather, pairs of levels

m and m' with the same "step number" N will do so at slightly different magnetic fields. Since the fourth order anisotropy has the same sign as the second order term, $(m^2 + m'^2)$ is bigger for levels m and m' lower in the double wells. Therefore, higher magnetic fields are required to bring lower levels into resonance. The direction of this correction will provide us with important hints in understanding the low temperature hysteresis data in Chapter 4.

Friedman *et al.* found in earlier hysteresis studies that the steps are nearly equally spaced in the regime of thermally assisted tunneling ($2K < T < 3K$) [10]. From our neutron scattering as well as Barra's EPR results, $A/D \approx 2 \times 10^{-3}$, and $(m^2 + m'^2)$ is not a very big number (less than 30) for levels near the top of the anisotropy barrier (in the case of thermally assisted tunneling, e.g. $N = 2$, $m = -4$, $m' = 2$) — their product is still relatively small and constitutes a correction of less than 6%. In addition, the broadening of resonance peaks by hyperfine/dipolar fields, as well as broadening associated with incomplete orientation of the powder samples, make it difficult for the effect of this small correction term to be visible in these experiments.

With the even finer energy resolution (27.5 μeV HWHM) of the Inelastic Neutron Scattering spectrometer at the Institute of Laue Langevin, France, Mirebeau *et al.* remeasured the low energy part of the spectra presented above and obtained very accurate values for the parameters of the spin Hamiltonian of Mn_{12} [56]: $D = 0.548(3)$ K, $A = 1.173(4) \times 10^{-3}$ K. With these parameters as well as g_z and C from EPR results by Barra *et al.*, a detailed energy diagram can be obtained through direct diagonalization of the spin Hamiltonian (Figure 2.6). Here, the 21 Eigen-energies of Mn_{12} are plotted as a function of longitudinal magnetic field (normalized by H_0).

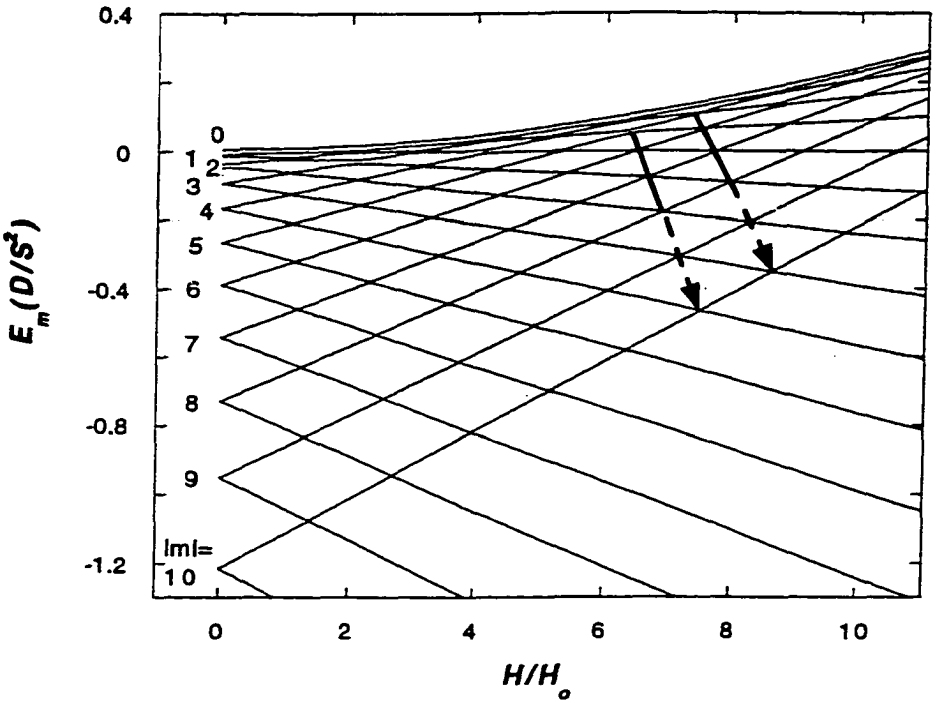

Figure 2.6: **Energy-level diagram obtained from diagonalization of the spin-Hamiltonian Eq. 2.2.**

Lines with positive slope correspond to negative quantum number m, and vice versa. The interesting physics occurs at the point where two lines "cross".[1] Magnetization tunneling occurs precisely at these "magic" points. The fact that these points do not collapse onto one point when projected on the x-axis (or field axis) is due to the fourth-order uniaxial anisotropy, $(-AS_z^4)$, as discussed above.

From Figure 2.6, it can be seen that this effect is small for small step number

[1]Strictly speaking, these are avoided crossings due to symmetry breaking terms in the spin Hamilonian.

N. In these conditions, the double wells are only slightly tilted. To match the experimental time, only tunneling relaxation near the top of the anisotropy barrier, i.e. thermally assisted tunneling, can be conveniently probed. As discussed above, it is fairly difficult to observe this change of less than 6%. However, in Chapter 3, a point-to-point measurement of the relaxation rate in Mn_{12} as a function of the longitudinal magnetic field reveals rich and complex structure due to this higher-order anisotropy.

For large values of N, this effect is substantial and can be more easily observed. Note that points at the crossings for a fixed step number N (e.g. $N = 8$) spread out over a wide range of magnetic field. The fourth-order term actually allows us to identify which level(s) is dominant in the tunneling relaxation by comparing the magnetic fields at which maxima of the measured relaxation rate occur with the calculated level crossings using the parameters in the spin Hamiltonian of Mn_{12}. This turns out to be a very powerful method (see Chapter 4).

The following chapters will show that this added complexity goes a long way toward helping us understand the intrinsic physics in Mn_{12}.

Chapter 3

Field-dependence of the Magnetic Relaxation in Mn_{12}-acetate in the Thermally Assisted Tunneling Regime

In this chapter, I will present results of point by point measurements below the blocking temperature of the magnetic relaxation of Mn_{12} which reveal unexpected, complex structure as a function of magnetic field applied along the easy axis of magnetization. This new form of spectroscopy yields detailed information about the tunneling process and the form of the spin Hamiltonian of Mn_{12}.

3.1 Motivation for a detailed study of relaxation

Compared to hysteresis measurements, studies of magnetic relaxation yield more straightforward results for the theoretical understanding of the tunneling process in Mn_{12}. Although measurements of steps in the hysteresis loops reveal the broad features discussed earlier, they do not provide the resolution or control necessary for a detailed study. In measurements of the hysteresis, the external magnetic field is swept continuously at some predetermined rate so that the magnetic response is generally probed only on short time scales [47]. For reasons that are only partially understood, the initial response of the magnetization in Mn_{12} is quite rapid and not characteristic of the long-time behavior of the relaxation [10]. We note also that there is a time-varying internal field associated with the time-varying sample magnetization which must be added to the externally applied field to obtain the total field $\mathbf{H}_{total} = \mathbf{H} + \alpha(4\pi\mathbf{M})$, where α is a unitless constant between 0 and 1 depending on sample details. The transient conditions of a hysteresis measurement make it particularly difficult to take this effect into account.

In relaxation measurements, the sample is cooled to the target temperature in some external magnetic field (zero in this study), and then the field is switched to another value. The decay of the sample magnetization towards its new equilibrium value is measured as a function a time. Since the (final) external magnetic field is fixed, this type of measurements provides a much more controlled way to study the relaxation process in Mn_{12} in comparison to a hysteresis study in which both external magnetic field and the sample magnetization are varying. The most accurate results are obtained by using single crystal samples.

3.2 Measurement techniques

All our Mn_{12} and Fe_8 single crystal samples were synthesized according to the published procedure [7] by David Hendrickson's group at the University of California, San Diego. These samples degrade on a time scale of months at room temperature. In order to slow this process, samples were stored in airtight containers in a freezer.

Choosing good single crystals is crucial to making good relaxation measurements. A batch of millimeter size single crystals of Mn_{12} were inspected carefully under an optical microscope and several selection criteria were applied. Parallelepiped crystals with shiny surfaces and sharp surface boundaries are considered to be good candidates. Crystals with irregular shape and cracked surfaces should be discarded. Both Mn_{12} and Fe_8 single crystals are very fragile so they should never be handled with tweezers or any other rigid handler. A sharpened Q-tip end with a tiny amount of non-magnetic grease (e.g. Dow Corning high vacuum grease, Lake Shore Cryogenics) can serve as a convenient "finger" to manipulate such single crystals.

DC magnetization measurements were performed using a Quantum Design MPMS-5 magnetometer equipped with a 5.5 T superconducting magnet. Single crystal samples were mounted on a Quantum Design horizontal sample rotator which allows rotation of the easy axis of the single crystal with respect to the magnetic field in increments as small as 0.1°. The in-plane orientation of the single crystal (defined by the angle ϕ in Figure 3.1) was achieved by applying a 1 Tesla magnetic field to tilt its c-axis towards the field direction [1] at room temperature ($\approx$ 300 K) when the rotator plate is roughly parallel to the field. After cooling the sample to below nitro-

[1] There is a thin layer of grease between the single crystal and the sample plate.

gen temperature (77 K), the in-plane rotational degree of freedom was frozen at its best value and the angle between field and c-axis was controlled solely by the sample rotator [2].

Two SQUIDs allow separate measurements of the two orthogonal components of the crystal's magnetization parallel and perpendicular to the field direction. The easy axis of the Mn_{12} single crystal was aligned parallel to the field by adjusting the angle θ between them to yield minimum perpendicular component of the magnetization in a field of 1 kOe at a temperature of 5 K (i.e. when the crystal is in the superparamagnetic regime). A ratio between perpendicular and parallel SQUID readings smaller than 10^{-3} was usually achieved. The largest unintentional transverse field due to this misalignment in the maximum 20 kOe longitudinal field used in our experiments is estimated at 20 Oe; compared with the estimated strength of $\approx$ 500 Oe of the hyperfine field [33], this has a negligible effect on the tunneling rate. After cooling the sample from 5 K to a target temperature T below the blocking temperature T_B in zero magnetic field, a fixed (longitudinal) field H_z was rapidly applied (in less than 300 s) and the magnetization of the single crystal was measured (by both SQUIDs) as a function of time. The excellent alignment of the single crystal was further confirmed by the fact that the small ratio mentioned above remained approximately the same throughout the entire relaxation. The relaxation measurement was repeated at a series of different fields and temperatures to span the relaxation conditions of interest. Since the magnetic relaxation depends strongly on temperature in the regime of thermally-assisted tunneling, the DC relaxation measurements we performed were limited to the field range between $0 - 20$ kOe and to the temperature range between

[2] Friedman's Ph.D. thesis provides a comprehensive and clear explanantion of the same MPMS-5 system, including principles of SQUID magnetometry and the low temperature sample rotator calibration. See ref. [19]

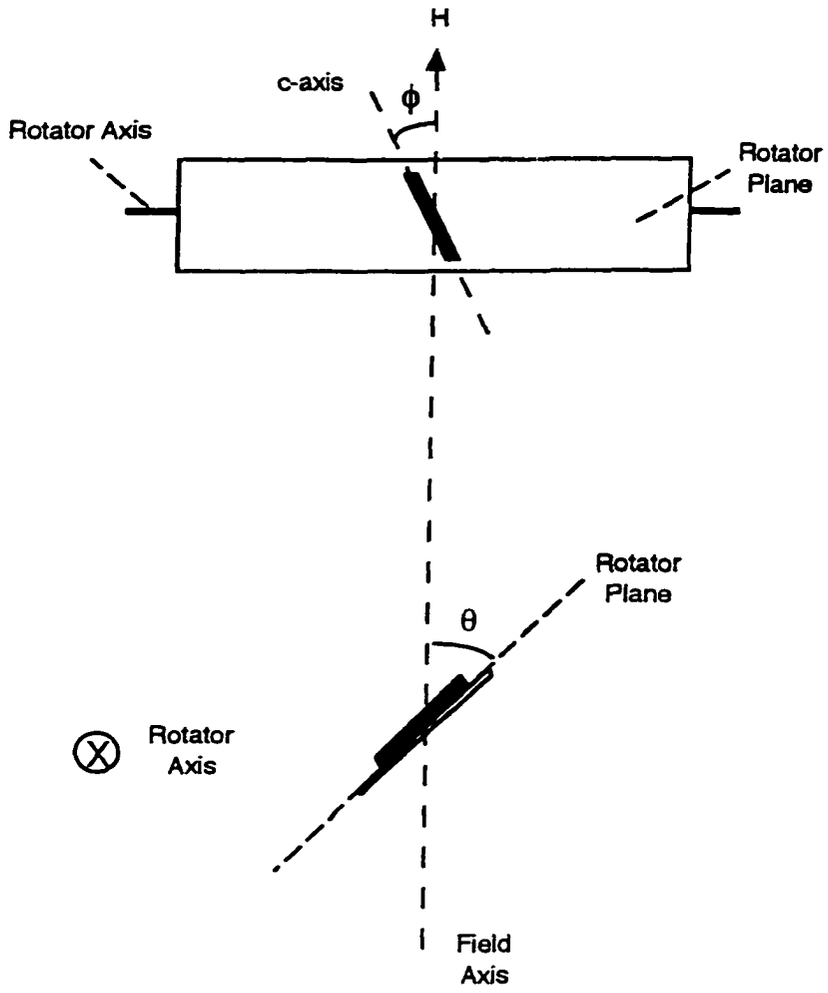

Figure 3.1: **Diagram showing the geometry of Mn_{12} single crystal and rotator plate. θ is the angle between field and rotator plane. ϕ measures in-plane orientation of the single crystal. A large field tilts the single crystal's c-axis towards its direction, therefore minimizing ϕ. θ can be minimized by rotating the plate.**

1.8 – 2.6 K in which a substantial portion of the relaxation can be measured on an experimentally convenient time scale to yield accurate relaxation rates.

3.3 Experimental results

It is a non-trivial task to extract a characteristic time (or rate) from these relaxation curves that unambiguously represents intrinsic physics which is comparable from curve to curve. For Mn_{12}, the relaxation of the magnetization is different in different regimes of temperature and in different time windows. At low temperatures, a square-root-of-time dependence at short time scales has recently been calculated [48] and claimed experimentally [49, 50], and attempts have been made to fit low-temperature relaxation data to this function to explore novel physics [49, 51]. However, at higher temperatures, measurements show that a faster process dominates the relaxation during an initial time period of about two thousand seconds (or less), followed by a slower relaxation which can be fit very well to a single exponential function, indicating that all the fast processes have died out [10, 19, 35]. Following our previous method of data analysis, it is this long time relaxation from which we obtain the characteristic rate by fitting it to a single exponential, as shown in Fig. 3.2. Note that the overall change in magnetization is small after about 2000 s, corresponding to a negligible change in the average internal field $\alpha(4\pi M)$ compared to the sizable (fixed) external field H. In our data analysis, we always fit a subset of data from the whole relaxation curve which satisfies this condition.

The relaxation rates at several different temperatures between 1.8 K and 2.6 Kare

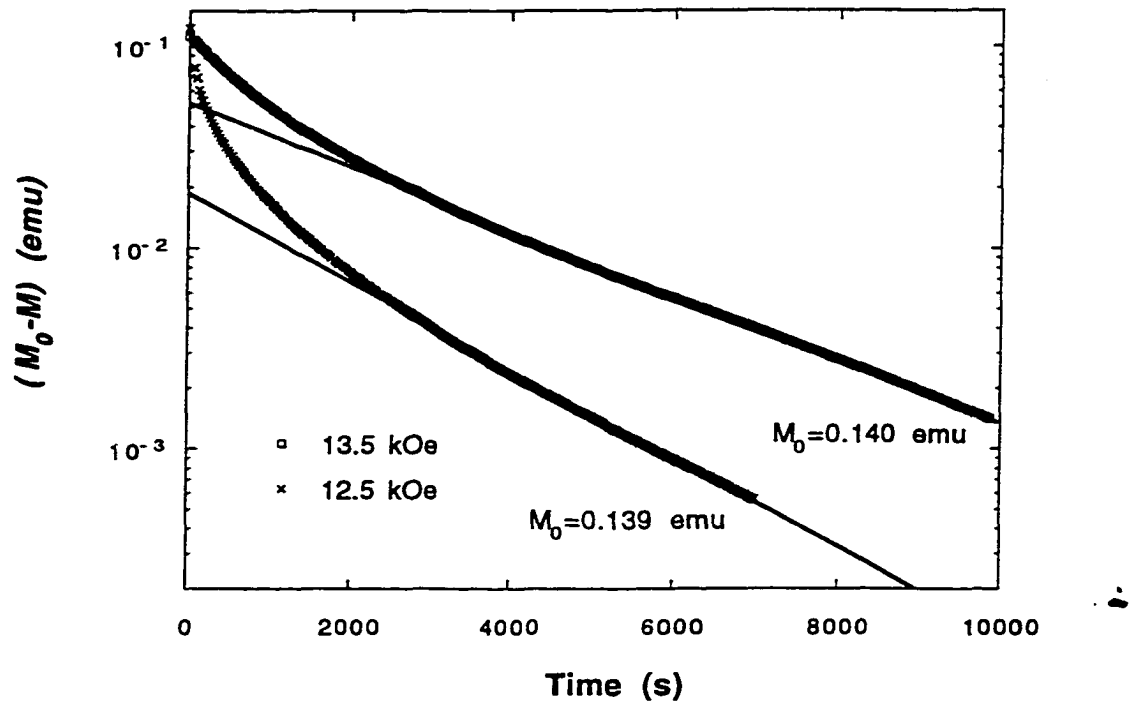

Figure 3.2: **The difference between the magnetization M and its equilibrium value M_0 vesus time on a semilogarithmic plot for a single crystal of Mn_{12}. The sample was cooled to 2.2K in zero field and then exposed to a field of 12.5 and 13.5 kOe applied along the easy axis of magnetization. The straight lines are fits to an exponential function for time $t > 2000$s. The inset shows the (spin-) potential for Mn_{12} in the presence of a longitudinal magnetic field.**

plotted in Figs. 3.3 and 3.4 as a function of the total longitudinal magnetic field $H_{total} = H + \alpha(4\pi M)$; the first term is the externally applied field H and the second term is the internal contribution due to the sample's magnetization. Here we used $\alpha = 0.57$ obtained from earlier measurements by Friedman [19] on similar samples.

Several observations can be readily made from the data. (1) The main features of the Γ vs.H_z curves confirm the results obtained from hysteresis measurements: there is faster relaxation at approximately regularly spaced values of the magnetic field. Within this range of temperature five peaks or resonances are observed, labeled by "step numbers" $N = 0, 1, 2, 3, 4$. (2) Some of the resonance peaks corresponding to the "steps" in the hysteresis loops exhibit additional internal structure. Most noticeably, the $N = 2$ and $N = 4$ peaks split into two or more small peaks at the higher temperatures. The $N = 1$ and $N = 3$ resonances have much simpler structure. However, a careful examination of the $N = 3$ resonance at $T = 2.20$ K reveals that it also consists of two closely spaced peaks. The $N = 0$ peak exhibits no apparent structure at the temperature of 2.60 K of our measurement, or at other temperatures measured earlier [23]. (3) Unlike most spectra, which generally become sharper and more detailed as the temperature is reduced, it is interesting to note that the structure is more complex at higher temperatures. This is particularly clear for the $N = 4$ resonance where three maxima are clearly seen at 2.00 K, while only one major peak (probably with a small right shoulder) is present at 1.80 K. (4) The separation of approximately 0.10 T between two neighboring peaks of the $N = 4$ resonance is twice as large as in the case of the $N = 2$ resonance, where it is about 0.05 T (see the $T = 2.00$ K and 2.47 K curves, respectively).

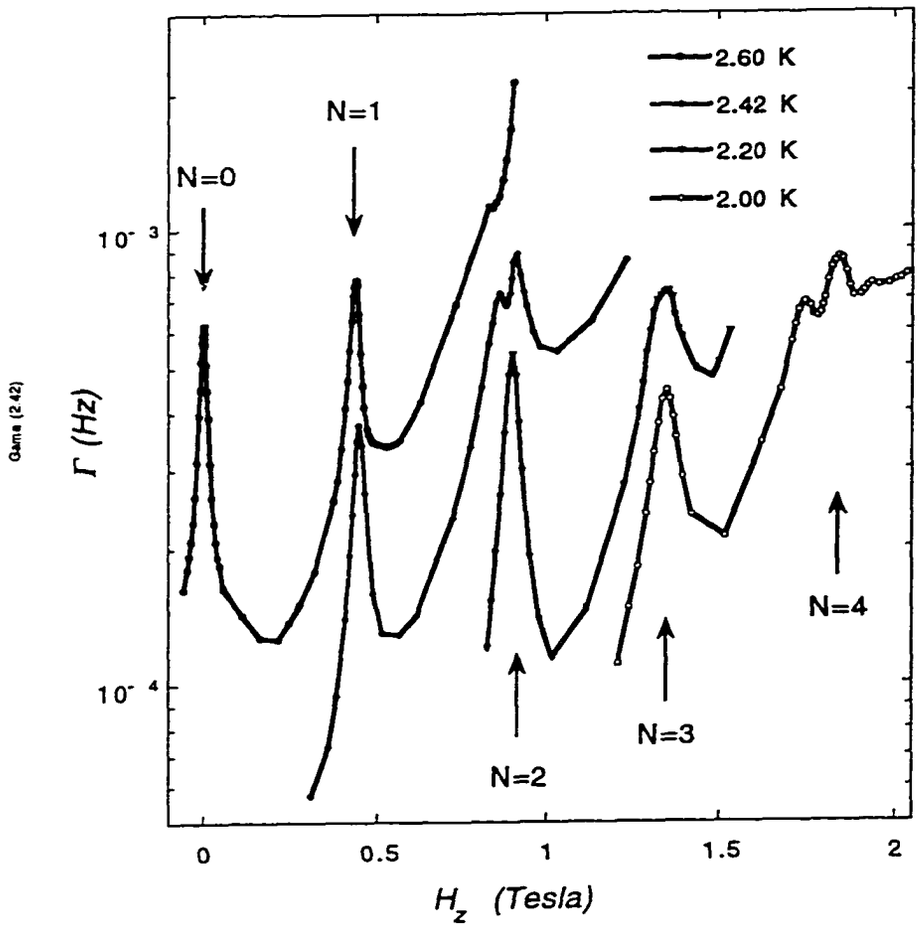

Figure 3.3: **Relaxation rate as a function of magnetic field H_{total} applied along the easy axis of a single crystal of Mn_{12}. Here $H_{total} = H + \alpha(4\pi M)$ with $\alpha = 0.57$.**

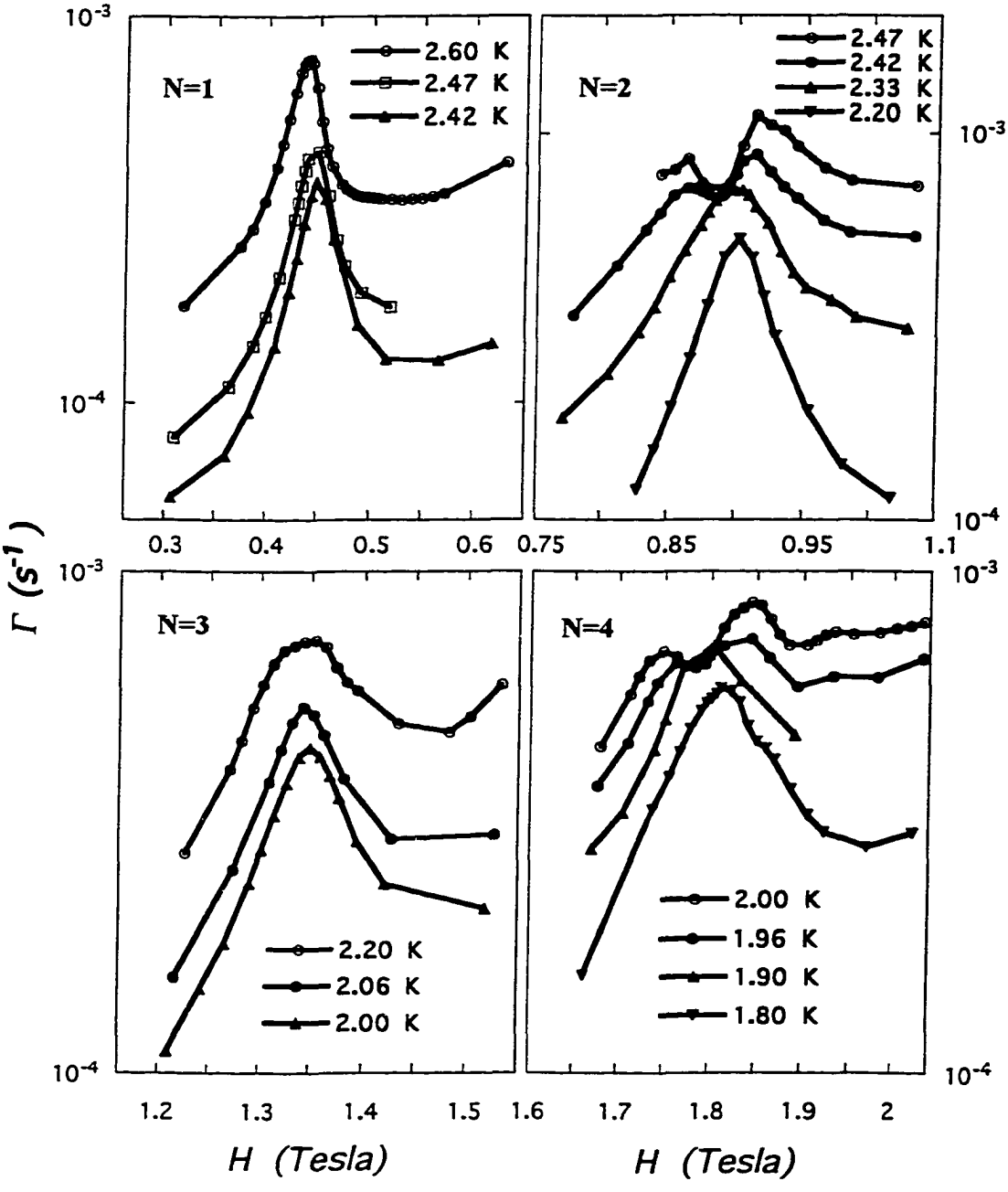

Figure 3.4: **Relaxation rate at several temperatures as a function of longitudinal magnetic field, displaying detailed structure within the $N = 1$, $N = 2$, $N = 3$, and $N = 4$ resonances.**

3.4 Discussion

Hysteresis and earlier relaxation studies of Mn_{12} indicated relatively simple structure in the form of a series of clean steps, each due to energy coincidences of a pair of levels (corresponding to spin projections) on opposite sides of the anisotropy barrier. In contrast, our detailed studies reveal that each resonance corresponding to a step displays rather complex structure. These spectra contain detailed information concerning the energy structure of the magnetic sublevels in each well and/or the tunneling process itself.

The observed structure could be caused by splitting by internal dipolar or hyperfine fields of individual spin states within each potential well. Recent experiments have shown that dipolar fields play a negligible role [34]. On the other hand, the hyperfine fields associated with the 5/2 spin of the Mn nuclei have been estimated at about $300 - 500$ Oe [33], so that each level with magnetic quantum number m is broadened (or split) into $\approx 2.2 \times 10^9$ nearly continuous sublevels. However, the structure we observe would require a complex energy distribution which would be difficult to justify. It is suggested instead that the spectroscopic features arise from the fact that different pairs of magnetic sublevels on opposite sides of the anisotropy barrier do not cross simultaneously, so that tunneling takes place at slightly different values of the magnetic field, as shown in the previous chapter.

Let us recall the Hamiltonian of Mn_{12} up to fourth-order terms: $\hat{\mathcal{H}} = -DS_z^2 - \mu_B \mathbf{H} \cdot \mathbf{g} \cdot \mathbf{S} - AS_z^4 + C(S_+^4 + S_-^4)$ which determines that a level in the metastable potential well with magnetic quantum number m comes into resonance with level m' in the stable well at a longitudinal magnetic field H given by: $H_z = N\frac{D}{g_z \mu_B}\left[1 + \frac{A}{D}(m^2 + m'^2)\right]$.

As a consequence, different pairs of levels m, m' on opposite sides of the anisotropy barrier come into resonance at slightly different magnetic fields for the same step number $N = \mid m + m' \mid$. Note that higher fields are necessary to bring lower-energy pairs (bigger $\mid m \mid$) into resonance, an effect that is more pronounced for peaks with higher numbered steps (due to the multiplicative factor N in the above equation). The exact amount of this non-simultaneuous crossing was calculated in Table I with parameters D, A, g_z from Electron Paramagnetic Resonance and Inelastic Neutron Scattering studies.

	$N=1$		$N=2$		$N=3$		$N=4$	
m	m'	H (T)	m'	H (T)	m'	H (T)	m'	H (T)
−1	0	0.422	—	—	—	—	—	—
−2	1	0.425	0	0.848	−1	1.275	—	—
−3	2	0.432	1	0.859	0	1.286	−1	1.719
−4	3	0.443	2	0.877	1	1.308	0	1.740
−5	4	0.458	3	0.902	2	1.340	1	1.776
−6	5	0.476	4	0.935	3	1.383	2	1.827
−7	6	0.497	5	0.974	4	1.437	3	1.891
−8	7	0.522	6	1.021	5	1.502	4	1.971
−9	8	0.551	7	1.075	6	1.578	5	2.064
−10	9	0.584	8	1.137	7	1.664	6	2.172

Table 3.1: Calculated values of magnetic fields at which a level m in the metastable well is in resonance with level m' in the stable well, from Eq. reffield. Values for parameters $D = 0.548(3)$ K, $A = 1.173(4) \times 10^{-3}$ K, and $g_z = 1.94(1)$ are taken from recent neutron scattering and EPR experiments.

Several features of the observed spectra are consistent with this model. As expected, the separation between the small neighboring peaks within the $N = 4$ resonance is generally larger than that between the $N = 2$ peaks, there is no substantial splitting (or shift) for the $N = 1$ resonance, and none at all for $N = 0$. Moreover, since the tunneling is thermally assisted in this temperature regime, one might expect that spin reversal through resonant levels near the top of the potential will become more active, introducing additional channels for tunneling as the temperature is raised. This could account for the fact that more complex structure is observed at higher temperatures. Quantitative comparison of the measured peak positions and the calculated resonant fields listed in Table I requires a reliable determination of the value of α used to calculate the total field $H_{total} = H + \alpha(4\pi M)$. Using $\alpha = 0.57$ found in earlier experiments on similar material[19], we suggest that the $N = 1$ peak centered at about 0.437 T at 2.60 K is associated with tunneling from $m = -3$ and/or -4 in the metastable well, while at the lower temperatures of 2.47 K and 2.47 K, the $N = 1$ maximum observed at 0.446 T is very close to the field 0.443 T listed in Table I for tunneling from $m = -4$ to $m' = 3$.

Other features of the data are more difficult to understand and warrant further discussion. One is that there appears to be considerably more structure in even ($N = 2, 4$) than in odd ($N = 1, 3$) resonances within the range of field and temperature of our measurements. It is puzzling, for example, that the $N = 3$ peak shows much less structure than the $N = 2$ resonance (note the multiplicative factor N of Eq. (1)). A second interesting feature is that the splitting within the $N = 2$ and $N = 4$ steps are too large to correspond to the difference in magnetic fields for two immediately neighboring level crossings (*i.e.* tunneling from m and $(m-1)$). Instead, they correspond more closely to the field difference for every *other* level crossing (*i.e.*

tunneling from m and $(m-2)$). In constrast, the $N = 3$ resonance has negligible splitting and its two closely-merged peaks are probably due to immediately neighboring level crossings. These effects suggest that higher-order transverse anisotropy is important in the tunneling process.

Two symmetry-breaking terms that could be responsible for tunneling have been considered: (1) a transverse magnetic field (of hyperfine/dipolar origin, or externally applied); and (2) an anisotropy term of the form $C(S_+^4 + S_-^4)$, the lowest order allowed by the tetragonal symmetry of Mn_{12}. Our data present a clear enigma. On the one hand, the odd-even asymmetry between steps and level-skipping within even-numbered steps both suggest that transverse anisotropy is responsible for the tunneling. On the other hand, the odd and even-numbered resonances have comparable amplitudes, albeit at different temperatures. This implies that the tunneling is due to transverse magnetic fields.

A simple calculation based on the model Hamiltonian as in Chapter 2 (Eq. 2.2) has been made. Assuming a (static) transverse magnetic field of 500 Oe consistent with former estimates [33], and using $C = 2.9(7) \times 10^5$ K derived from experiment[24], we calculated the tunnel splittings by diagonalizing the 21×21 matrix representing the spin Hamiltonian of Mn_{12} of Eq. (1). The tunnel splittings, $\Delta_{m,m'}$, thermal population factors, $e^{-E_{m,-10}/kT}$, and the tunneling probabilities obtained from the product of thermal population factor and tunnel splitting squared, are listed in Table 3.4 for several pairs of levels (m, m') within steps $N = 1$ and $N = 2$. Unfortunately, the results do not produce the right ratio of amplitudes between these peaks for *any* values of the parameters: the odd-even asymmetry requires that transverse anisotropy dominate, while the comparable amplitudes require that a transverse field be the dominant symmetry-breaking term. Which mechanism is responsible for tunneling in

this material is an interesting question that has yet to be resolved.

—	m	m'	$\Delta_{m,m'}$ (K)	$e^{E_{m,-10}/kT}$	$\Delta^2_{m,m'}e^{E_{m,-10}/kT}$ (K^2)
$N=2$ $T=2.42$ K	−4	2	3.7×10^{-2}	8.41×10^{-10}	1.15×10^{-12}
	−5	3	3.8×10^{-2}	5.11×10^{-9}	7.30×10^{-12}
	−6	4	2.4×10^{-4}	5.62×10^{-8}	3.24×10^{-15}
	−7	5	1.9×10^{-4}	1.17×10^{-6}	4.22×10^{-14}
$N=1$	−5	4	5.1×10^{-3}	6.29×10^{-9}	1.63×10^{-13}
$T=2.60$ K	−6	5	1.5×10^{-5}	7.11×10^{-8}	1.60×10^{-17}

Table 3.2: Resonant tunnel splittings calculated through Eq. 2.2, $\Delta_{m,m'}$, the Boltzmann factor, $e^{E_{m,-10}/kT}$, and the tunneling probability p given by the product of $\Delta^2_{m,m'}$ and $e^{E_{m,-10}/kT}$ are shown for several pairs of levels (m,m'). Here $D = 0.548(3)$ K, $A = 1.173(4)\times 10^{-3}$ K, $g = 2$, $H_x = 500$ Oe, $C = 2.9(7)\times10^{-5}$ K. This simple calculation does not produce the right ratio of amplitudes between peaks (not even on the correct order of magnitude). Note that relative to the $N = 2$ resonances, the $N = 1$ resonances are at least an order of magnitude smaller.

Leuenberger and Loss [38] and Pohjola and Schoeller [39] recently presented a comprehensive theory of the magnetization relaxation in Mn_{12} in the thermally assisted tunneling regime. The relaxation rate as a function of longitudinal magnetic field was calculated using a Hamiltonian that includes spin-phonon interactions, quartic magnetic anisotropy and a weak transverse field. They obtained satellite peaks qualitatively similar to those shown in Figs. 3.3 and 3.4 whose amplitude and width they investigated [38] for various angles between the sample easy axis and the field direction. Quantitative agreement between their theory and our experimental observations requires a substantial transverse magnetic field, due perhaps to mosaic spread

or unintentional misalignment of the sample with respect to the magnetic field direction. However, the mosaic spread of approximately 0.4 degrees [29] found for Mn-12 crystals is too small to account for our observations, and the degree of misalignment required to give a sufficiently large transverse component is well outside our experimental margin of uncertainty and would yield different results each time a sample is mounted and aligned.

To conclude this chapter, we note that the point-by-point relaxation measurements presented in this paper represent a novel form of spectroscopy. "Spectra" obtained from such measurements allow detailed studies of the tunneling process, and provide important information regarding the dominant tunneling paths at different temperatures and magnetic fields.

Chapter 4

Magnetic Relaxation Study of Mn_{12}-acetate below 1 K.

A powerful measurement technique combining micron-scale Hall-effect magnetometry and sub-millimeter single crystals of high-spin molecules has been developed to enable the study of magnetization tunneling in these materials at temperatures below 1 K. This work was initiated in collaboration with Andrew Kent and Louisa Bokacheva in the laboratory of Professor Kent at New York University, and then continued at City College using Hall bars provided by Professor Eli Zeldov of the Weizmann Institute. In this chapter, I shall first list the many advantages of micron-scale Hall Magnetometry in comparison with other low temperature magnetic measurement techniques. I will then describe in detail the experimental procedure. Finally, I will present experimental data for the magnetic relaxation of Mn_{12} down to 0.4 K from our first successful run based on this method. Our data reveal a sharp transition from thermally assisted to ground state tunneling which will be interpreted in light of the recent theory by Chudnovsky and Garanin [14].

4.1 Background on Hall magnetometry

In our study, the motivation to use Hall magnetometers to investigate Quantum Tunneling of Magnetization originated from strong interest in tracing the properties of thermally assisted tunneling in Mn_{12} down to temperatures below 1.7 K available in commercial SQUID magnetometers [31]. The higher-numbered steps have progressively faster magnetic relaxation because the anisotropy barrier is lowered by the applied field. Therefore, measurements at lower temperature are needed to observe them. For example, it has been estimated that "step numbers" up to $N = 19$ should be observed with the temperature reduced to near 10 mK. However, it is difficult to attain such low temperatures using SQUID techniques in standard commercial devices. Relative motion between the sample and the detection coils, a standard technique applied in almost all contemporary SQUID magnetometers, makes it extremely difficult to maintain low temperatures. A Hall probe does not involve mechanical motion and can be easily anchored to the coldest part of a cryostat, thus making it a good candidate for low temperature studies of high-spin molecules.

Hall magnetometry has been developed in recent years as a powerful technique to measure magnetic properties of small particles [57, 58]. Classically, it is well known that the transverse Hall voltage generated in a long strip geometry of thickness t in the presence of a magnetic field B normal to the Hall bar plane is given by:

$$V_H = \frac{IB}{qtn_{3D}} \tag{4.1}$$

where I is the current, n_{3D} is the 3-dimensional carrier density and q is the carrier charge. Since V_H is proportional to both the current I flowing through the Hall bar and the magnetic field B, the Hall coefficient can be defined as,

$$R_H = \frac{V_H}{IB} = \frac{I}{qtn_{3D}} \tag{4.2}$$

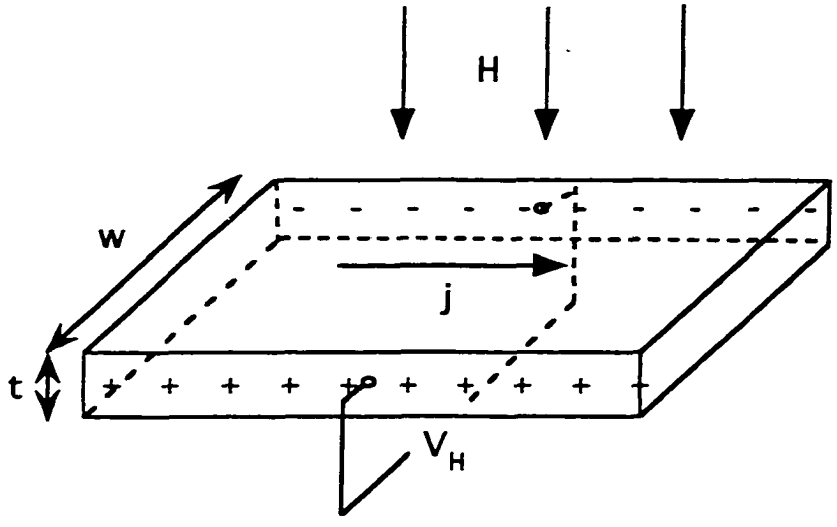

Figure 4.1: **Diagram of the classical Hall effect. A Hall voltage (V_H) is present when the Lorentz force from the magnetic field on the drifting electric carriers is balanced by the static Hall (electric) field on the same carriers. This method also yields a powerful experimental tool in understanding many important phenomena in modern physics.**

which measures a Hall bar's capability to transform a (small) magnetic field into a (large) Hall voltage at a specific working current I.

The Hall bar technique is straightforward to apply because of the near linearity of the Hall signal over a wide range of magnetic fields and temperatures (in which quantum effects play a negligible role). The magnetic signal can therefore be easily obtained from the measured Hall voltage by simply making a linear transformation.

As with SQUIDs, Hall probes can be configured as gradiometers, enabling high sensitivity measurements in large externally applied magnetic fields. This important feature makes it possible to measure the (relatively small) magnetization change (for Mn_{12}-acetate, $4\pi M$ at saturation is about 600 Gauss [19]) in the presence of a large external field which is usually of the order of several Tesla.

In a usual SQUID measurement, the sample flux is transferred via a superconducting pick-up coil to the input coil of the SQUID. However, this technique is unsuitable for the study of submillimeter size single crystals since the spatial separation of pick-up coil and SQUID leads to a very small coupling factor. In a Hall bar measurement, the single crystal can be coupled very closely (within several microns) to the Hall sensor area. Further, the size of the probe can be easily matched to the samples and the experimental space. For small samples, micron sized probes can be fabricated, resulting in a large flux filling factor which can significantly improve the coupling of flux to the sensor to result in a high sensitivity.

In addition, Hall devices operate over a much wider range of applied field and temperature than a SQUID. SQUIDs, usually fabricated from Nb-AlO_x-Nb layers,

are superconducting only within a certain range of field and temperature. For Hall bars, the applied field and temperature range can be substantially extended in which high spin molecules can be studied in great detail.

In short, Hall bars are a valuable tool for the measurement of magnetization at low temperatures because of their ease of use, high sensitivity, and wide temperature and field range.

The choice of sensor material and thickness can critically influence the performance of a Hall bar, as is clear from Eq. 4.1. Two types of Hall sensor materials have been commonly used for the purpose of magnetometry: the first type is high mobility 3D bulk (or thick films) of semiconductors (such as InGaAs) and the second type is high mobility 2D heterostructure (such as GaAs/AlGaAs). A rough estimate from the knowledge of carrier densities in these materials[1] yields the following typical values of the Hall coefficients: $R_H = 0.1\ \Omega$/Gauss for a 2D sample compared with $R_H = 0.1$ mΩ/Gauss for a 3D bulk semiconductor (at 1 μm thickness). Higher current is necessary to produce the same voltage response in 3D materials, resulting in greater power dissipation, and consequently heating, to the sample as well as larger unwanted sensor self-fields.[2] Clearly, 2D heterostructures are typically three orders of magnitude better than 3D semiconductors in transforming a small magnetic signal from the sample into a substantial Hall voltage. In this Chapter, my discussions will be related to 2D Hall bars only.

---

[1] In a 2D system tn_{3D} evaluated at $t \to 0$ becomes the 2D carrier density n_{2D}.

[2] The small local magnetic field generated by the working current I can be measured by the Hall bar itself and should therefore be minimized.

4.2 Measuring magnetization with Hall bar magnetometers

2D Hall bars from two different sources were used in our studies. One type of Hall bar is from Professor Andrew Kent at New York University. It is a high mobility GaAs/GaAlAs 2D hole gas sample with carrier density $n_{2D} = 3 \times 10^{11}$ cm^{-2} and mobility $\mu(5K) = 10^5$ cm^2/Vs. The linewidths for the current and voltage probes range from 1 to 10 μm and the hetero-interface is 100 nm below the surface. The other type of Hall bar is from Professor Eli Zeldov at the Weizmann Institute of Science, Israel. It consists of an array of microscopic Hall sensors realized in a 2D electron gas formed at a GaAs/AlGaAs interface as shown schematically in Fig. 4.2. The typical 2D electron density in these samples is around $n_{2D} = 5 \times 10^{11}$ cm^{-2} and similar mobility $\mu(5K) \approx 10^5$ cm^2/Vs. Zeldov's Hall bars enable high spatial resolution measurements on small crystals. Aside from their difference in carrier type and slight variation in carrier density, these two types of Hall bars share many basic features in their application as small Hall effect magnetometers.

4.2.1 Instrument preparation

A home-made current source ($I = 0.1-10$ μA, AC/DC) was used to generate a highly stable working current I flowing through the Hall bar. A diagram of the measurement setup is shown in Fig. 4.3. In its AC measurement mode, the current source receives an AC voltage input from a Lock-in Amplifier (Stanford Research Systems, Model SR850 DSP) and generates a highly stable current (at the same AC frequency) to the

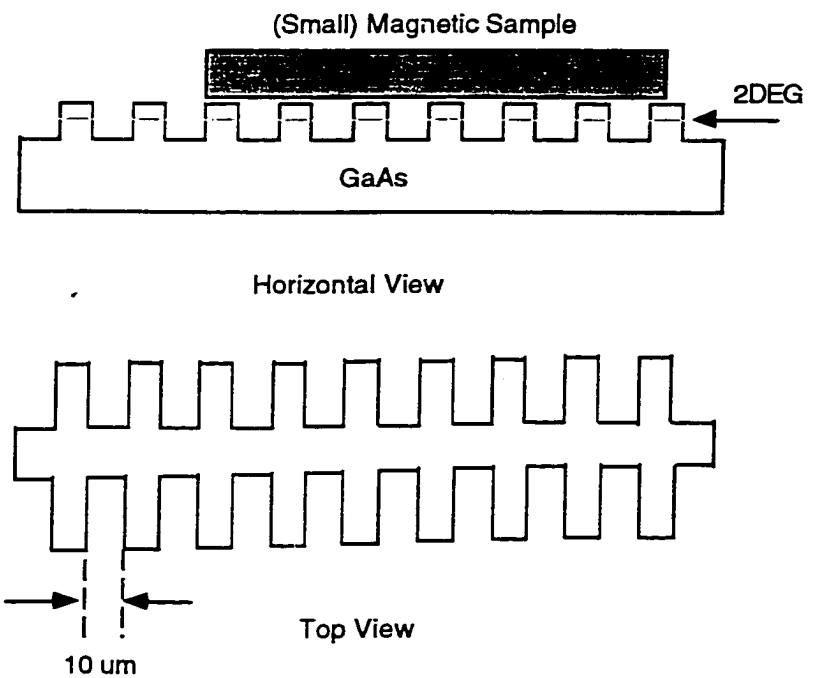

Figure 4.2: **Schematic diagram of the Hall sensors from Dr. Zeldov. It is shown as an array of GaAs/AlGaAs two-dimensional electron-gas Hall sensors with an active area of $10 \times 10\ \mu m^2$ and an even separation of $10\ \mu m^2$.**

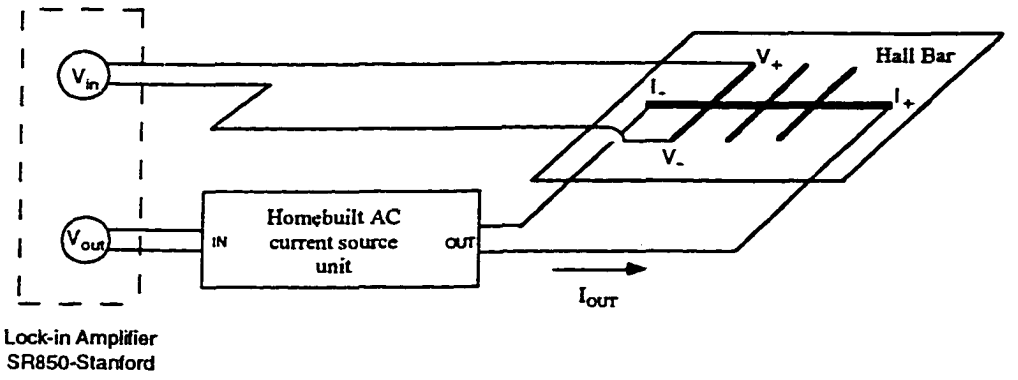

Figure 4.3: **Diagram of the Hall measurement set-up.**

Hall bar. The AC voltage is then fed into the Lock-in Amplifier to get time averaged integration to produce the final Hall voltage V_H. The fluctuation in current I from the current source is as small as 0.05% (or 0.5 nA at 1 μA). Careful attention was paid to reducing electrical noise by connecting rf filters to wires which go inside the He3 cryostat.

All Hall bar measurements were carried out in a He3 crystat which can cool the sample down to a much lower base temperature (typically 0.3 K) than a He4 cryostat. Oxford-Heliox, the He3 system used at City College has a top-loading sample probe equipped with a horizontal sample rotator with an acuracy to 0.1°. The Hall bar is mounted onto a home-made socket rigidly anchored in the space within the sample

rotator holder. In the experiment, the Hall bar on the probe is lowered into the Heliox insert, and cooled to its target temperature. Oxford-Heliox achieves a base temperature of about 240 mK, a substantial base temperature decrease compared to other He3 systems (It is always desirable to study pure ground state tunneling at an even lower temperature.) In addition, the cryostat is equipped with a 12 Tesla magnet which can produce a DC field even larger than the anisotropy field of Mn_{12}-acetate (10 T).

The Data Collection Software and GPIB User Interface (by LABVIEW) were expertly designed and tested by my colleague Kevin Mertes. The values of temperature T, magnetic field H, Hall voltage V_H, longitudinal resistance R_{xx}, and current I were automatically recorded during the experiment.

4.2.2 Hall bar characterization

The empty Hall bar needs to be well characterized *before* the sample is placed onto it. The characterization provides important information for the Hall bar such as its carrier density, mobility and temperature dependence. These numbers not only reflect the quality of a Hall bar, influencing our decision on whether to use it, but also provide a conversion table in later magnetization measurements to allow accurate conversion from measured Hall voltage to sample magnetization.

Hall bar plane perpendicular to magnetic field

Before a Hall bar is loaded into the insert of the Heliox cryostat, the Hall bar plane is aligned approximately perpendicular to the magnetic field, or the probe axis, by using the sample rotator. The experimenter should put down such important information as

the readings of the sample rotator when the Hall bar plane is (roughly) perpendicular and parallel to the field direction, and to which direction the Hall bar plane will rotate if the rotator knob at the top of the probe is turned clockwise or counterclockwise (top view). This seemingly trivial step should never be bypassed since a rotation of the Hall bar in the wrong direction (or over-limit rotation) could easily break a thin wire, wasting a lot of sample preparation time, and we have no way to obtain this information after the sample probe is loaded into the insert.

Two typical V_H vs. H curves measured in this perpendicular configuration at two different temperatures are shown in Fig. 4.4 for a Zeldov Hall bar. There is always a good linear part near $H = 0$, up to about 0.8 T. Quantum plateaus start to set in at about 1 Tesla. However, for reasons which will be discussed later, this non-linear deviation will not complicate the magnetization measurement. From the curve, the slope of the linear part near $H = 0$ can be obtained to get R_H. Several V_H vs. H curves at difference temperatures between 2 K and 0.24 K should be obtained to allow assessment of the temperature dependence of the Hall resistivity at low temperatures. For Hall bars provided by Zeldov, the change of slope with temperature near $H = 0$ is negligible below 1.7 K (see Fig. 4.4).

Hall bar plane parallel to magnetic field

The next step is to rotate the Hall bar plane into a position parallel to the magnetic field. The most convenient way to do this is to apply a large and constant magnetic field (typically 3-5 Tesla) and monitor the decrease of Hall voltage while rotating the Hall bar plane. Since the Hall voltage is only related to the perpendicular component of the (fixed) field $H_z = H \sin\theta$, a (near) parallel orientation can be achieved by reducing the Hall voltage (or more accurately, R_{xy}) to a value as close to zero as

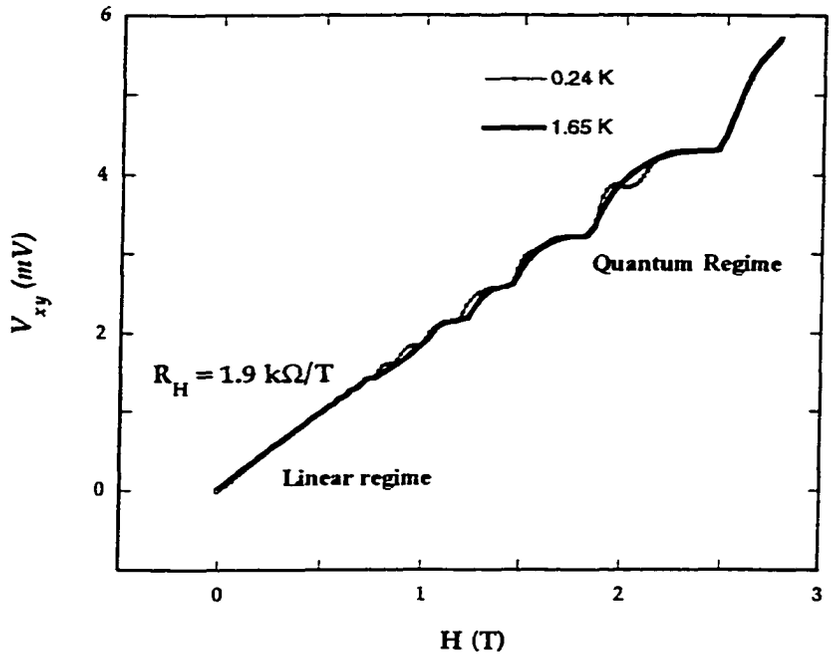

Figure 4.4: V_{xy} **plotted as a function of perpendicular magnetic field** H **at two widely different temperatures. The stable current used is** 1.00 μ**A. Two curves merge in the linear regime close to** $H = 0$ **and diverge in the quantum regime. However, this divergence is of neither interest nor importance to our Hall magnetometry.**

possible.

In this configuration, R_{xx} is measured as a function of magnetic field H. This step needs to be carried out for the following reason. Usually the voltage leads on a Hall bar are not perfectly symmetric (see Fig. 4.5), and the tiny misalignment of voltage leads can admix some R_{xx} component into the measured Hall voltage. This can create a very unsatifactory situation if R_{xx} has a strong field dependence which then introduces an unwanted large change in the measured Hall voltage which is totally unrelated to the magnetization change of the sample. Of course, due to the difference in symmetry for R_{xx} and R_{xy} as a function of field, a correct R_{xy} vs. H curve can always be obtained by separating these two components. However, this method will generate large experimental error. Knowledge of the R_{xx} vs. H curve for a Hall bar in this orientation minimizes the need for this separation procedure. Fortunately, for samples both from NYU and the Weizmann, R_{xx} is a smooth function of H (see Fig. 4.5). Therefore, even in a case when there is a slight misalignment of voltage leads in the Hall bar, it only contributes a near-constant shift to the measured voltage.

Further characterization could be applied such as measuring R_{xx} vs. H curves in the perpendicular orientation and R_{xy} vs. H curves in the parallel orientation. This will provide more detailed information on a Hall bar even though the two tests mentioned above should be sufficient for the purpose of using Hall bar as a low temperature magnetometer.

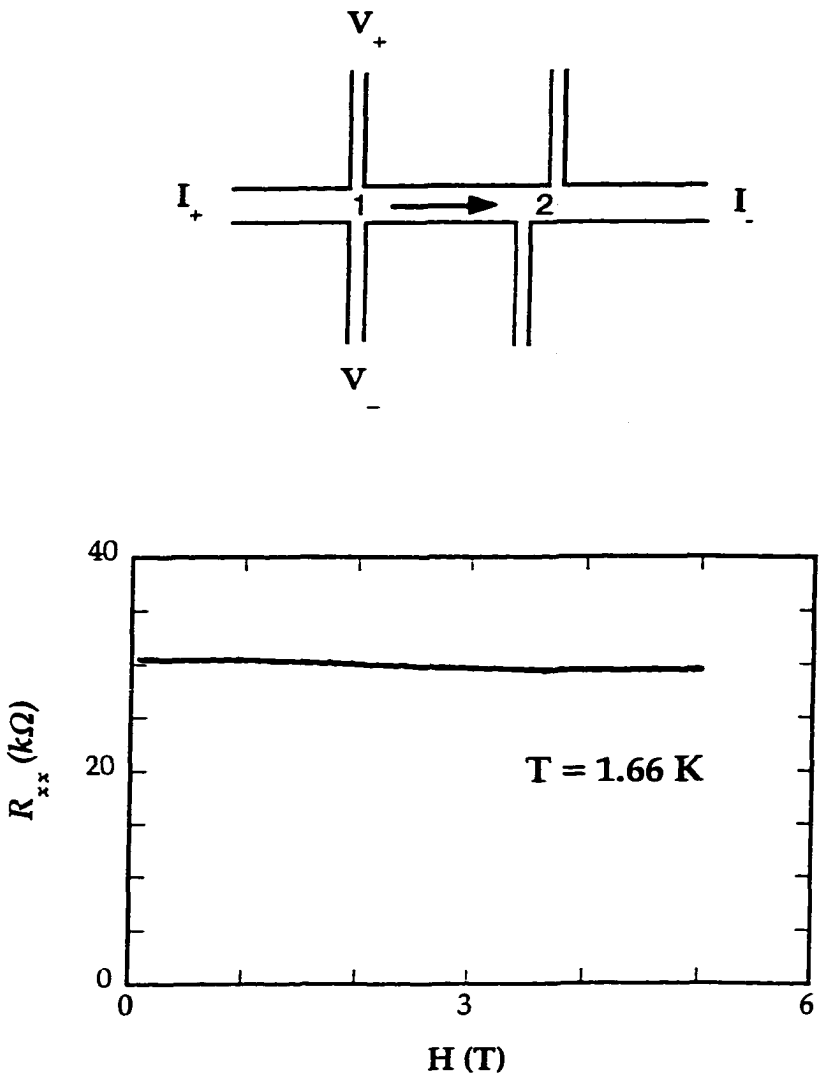

Figure 4.5: **Misallignment of voltage leads in a Hall bar (exaggerated in this diagram). This can introduce a large R_{xx} component into the measured voltage between two voltage leads. A typical R_{xx} vs. H curve is shown in the lower part of the same figure.**

4.2.3 Single crystal selection and magnetization "avalanches" at low temperature

The same method for choosing a good single crystal described in Chapter 3 can be applied here even though the crystal will be finally placed onto a Hall bar instead of a rotator plate. However, a major difference between magnetization measurements at temperatures above 1.7 K with a SQUID magnetometer and at lower temperatures with a Hall bar is the size of the single crystal sample used. In a SQUID measurement, bigger single crystals are highly desirable in order to yield bigger sample magnetization signals. Thermalization of the big crystal (usually with He4 gas at a specified temperature) is not a problem in this temperature range. However, at the lower temperature where Hall bar measurement were performed, single crystals one or two orders of magnitude smaller should be used. This size requirement is a direct consequence of difficulties in thermalizing the sample at low temperatures.

At lower temperatures, sample heating due to the so-called "avalanche" effect has made it hard to obtain clean results [17]: the magnetization of the sample abruptly switches to its saturation value with a sharp increase in sample temperature. Microscopically, this corresponds to a process of spin-phonon interactions with positive feed-back — without an effective way to transfer to the main bath the energy released after the spin reversal of some magnetic molecules, part of the energy remains in the sample and causes local heating which promotes more spins to reverse their magnetic moment, which in turn causes more heating, and so on. Unfortunately, avalanches are more likely to occur at lower temperatures due to the T^3-dependence of the crystals' heat capacity.

To overcome this problem, much smaller Mn_{12} single crystals (micrometer-sized to

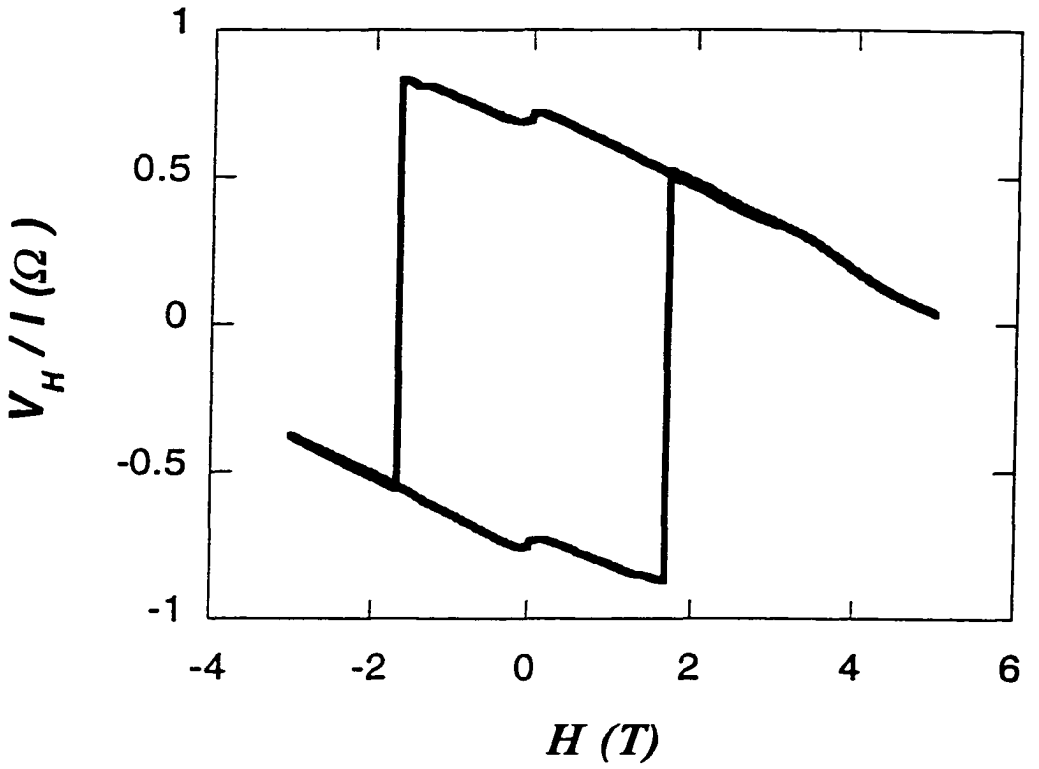

Figure 4.6: **Experimental data showing "Avalanche" of magnetization due to poor thermalization between sample and main bath.**

sub-millimeter) were used to maximize the surface-to-volume ratio to allow effective heat transfer. Accordingly, micron-scale Hall probes were needed to study the magnetic properties of these small samples. Careful attention was also paid to get better sample thermalization to the bath so that the heat generated during relaxation can be effectively carried away. The working current of the Hall bar was reduced to $\approx 1\mu$A to minimize power input from the measurement ciruit (and at the same time still maintain a good signal-to-noise ratio). After these careful improvements, temperature stability of the sample was finally achieved to allow a controlled low temperature study.

4.2.4 Making meausurements

A thin layer of non-magnetic low-temperature grease (of the same Lakeshore brand as mentioned in the last chapter) is applied on the surface of the Hall bar and a submillimeter Mn_{12} single crystal is placed on top of it. This configuration is pictured in Fig. 4.7 and illustrated schematically in Fig. 4.8. The square edge of the single crystal is positioned very close to one of the crossings between current line and voltage line to yield maximum flux coupling to the active area of the Hall bar. The c-axis of the single crystal can be easily recognized as the longest dimension of the parallelepiped, and its in-plane orientation is adjusted such that the magnetic field is parallel to the c-axis (with an error of several degrees) when the Hall bar plane is rotated into a parallel position with the magnetic field.

Before a measurement, the Hall bar plane is fine-tuned by the sample rotator to be parallel with the field. This orientation can be easily achieved by making sure that the Hall voltage doesn't change with magnetic field when the Mn_{12} single crystal is in its

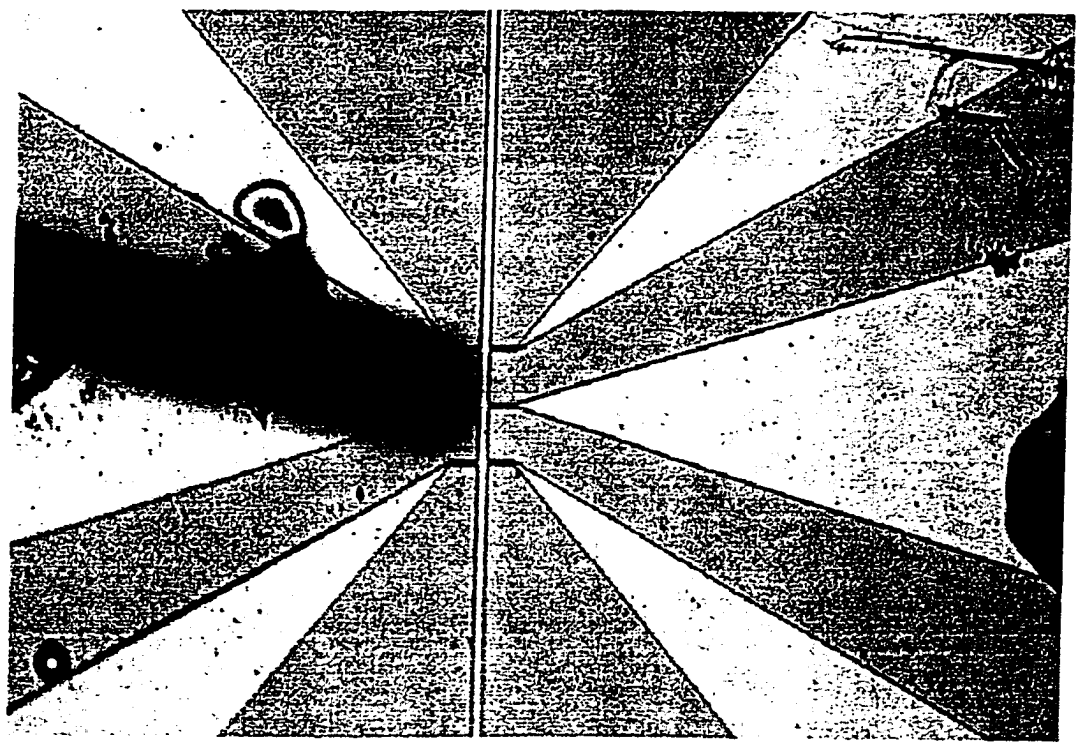

Figure 4.7: **FIG. 4.7: A photo of a Mn_{12} single crystal on Hall bar.**

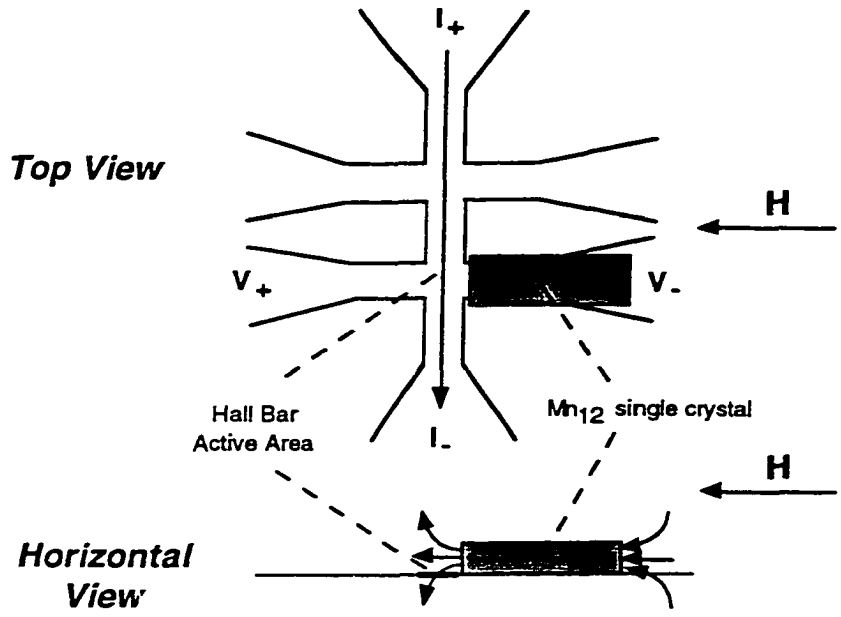

Figure 4.8: **Diagram of the experimental set-up of a typical magnetic moment measurement using micron-sized Hall bar at temperatures below 1 K.**

saturated state above the blocking temperature. In this configuration, the magnetic field has no perpendicular component to the Hall bar plane. Therefore, no matter how high the externally applied field, the Hall bar active area can only sense the flux generated by the single crystal sample. On the other hand, the magnetization of the sample can be influenced by the large magnetic field applied parallel to its c-axis. This cleverly chosen geometry effectively separates the sample's signal from that of the external field, yielding a highly sensitive magnetization measurement.

Therefore, the measured Hall voltage is only proportional to the coupled flux from the sample which is again proportional to the sample's magnetic moment.

$$V_H \propto R_H I \Phi_{sample} \propto R_H I(4\pi M). \tag{4.3}$$

By introducing a "coupling constant" α which measures the coupling between sample and Hall sensor area, the above equation can be rewritten as

$$V_H = \alpha R_H I(4\pi M) \tag{4.4}$$

α depends on many factors such as sample shape, edge distance to the sensor active area and the thickness of the grease. Typical values of α in our experiments are between 0.2 and 0.5.

For Mn_{12}, $4\pi M$ in the saturated state M_S has been estimated at about 0.06 Tesla [19]. For a typical Hall measurement in this study, $I = 1\mu A$, $R_H = 2k\Omega A^{-1}T^{-1}$, and $\alpha = 0.3$, this magnetic moment can be amplified into a sizable Hall voltage of $36\mu V$. With the stablity of the home-made current source, a field sensitivity of 0.2 Oe can be achieved for the Hall bar as a low temperature magnetometer. The above numbers demonstrate the capability of using Hall bars to study magnetization tunneling in Mn_{12}-acetate.

Since the maximum perpendicular component a Hall bar active area can sense is $\alpha(4\pi M_S)$ which is about several hundred Oe, only a very small portion near $H = 0$ in Fig. 4.4 is relevant in converting sample magnetization to Hall voltage. That is why I claimed that the existence of high field quantum plateaus does not affect the problem at all.

4.3 Low temperature magnetic hysteresis in Mn_{12}-acetate

Precise mganetization measurement of small single crystals of Mn_{12}-acetate were performed down to 0.4 K using high sensitivity Hall magnetometry as discussed above. Data analysis using the spin Hamiltonian with parameters determined by EPR and Neutron Scattering experiments (Chapter 2) reveals an abrupt, or first-order, transition between thermally assisted and pure quantum tunneling, as suggested by recent theory.

4.3.1 Extending hysteresis studies to low temperatures

The magnetization of small single crystals of Mn_{12} in the form of a parallelepipeds ($50 \times 50 \times 300 \mu m^3$) was measured using a micron-sized Hall magnetometer. Careful attention was paid to reducing electrical noise and to thermalizing the sample. The temperature was measured both at the cold stage of the cryostat and with a small resistance thermometer mounted within a few mm of the sample. These measurements were always within 50 mK of one another. Fig. 4.9(a) shows a typical portion of a hysteresis curve measured at 0.4 K starting from a demagnetized state, $M = 0$, and measured at a ramp rate of 0.1 T/min, with the field applied along the easy axis (within a few degrees). (Please note that the c-axis of a Mn_{12}-acetate single crystal is the same as the easy axis internal to the molecule). Prominent step-like changes in magnetization are observed at fields between 3 and 5 Tesla. The high quality of the data is evident from the large signal-to-noise ratio in the dM/dH versus H curve which has well-defined peaks, as shown in Fig. 4.9(b). Each peak corresponds to a step (faster relaxation) in the parent curve of M versus H, or a maximum in

the magnetization relaxation rate at that applied field, sample magnetization and measurement temperature. The peak positions provide accurate information about the magnetic field at which a level in the metastable well coincides with a level in the stable well. Indeed, a new type of "spectroscopy" measurement can be developed to study the details of this level matching picture to obtain essential physics of the system.

Fig. 4.10 shows the derivative of the magnetization curves dM/dH versus applied field H at different temperatures from 2.4 K to 0.4 K. First, above 1.6 K the data are in good agreement with previous experiments. Peaks appear at approximately equally spaced field intervals ($\sim$ 0.45 T) and their amplitude is a strong function of the temperature. As the temperature is reduced, higher numbered maxima in dM/dH appear, while lower field peaks decrease in amplitude, again, consistent with the model of thermally assisted tunneling. Second, on lowering the temperature, the peaks shift continuously to higher fields. For instance, peak $n = 5$, at 2.2 K is at 2.2 T and by 1.4 K it has shifted to 2.33 T. Third, and most intriguing, at low temperature ($T < 1.2$ K) peaks in dM/dH shift dramatically in position as a function of temperature. This is well illustrated by the behavior of the $n = 7$ peak as the temperature is reduced. This peak first appears at 1.6 K at $H = 3.10$ T, grows in amplitude and shifts to significantly higher fields on lowering the temperature and, at 1.0 K, abruptly develops a high field shoulder. On slightly lowering the temperature to 0.9 K, "spectral" weight is transferred into this shoulder and at the lowest temperature the peak remains fixed in position. This peak has shifted to 3.53 T, by nearly a full field quantum H_0, in this temperature interval. Shifts in peaks positions of this order are seen for all the steps observed at low temperature ($5 \leq n \leq 9$). Finally, note that at 0.6 K and lower temperature, the maxima remain fixed in field and approximately constant in

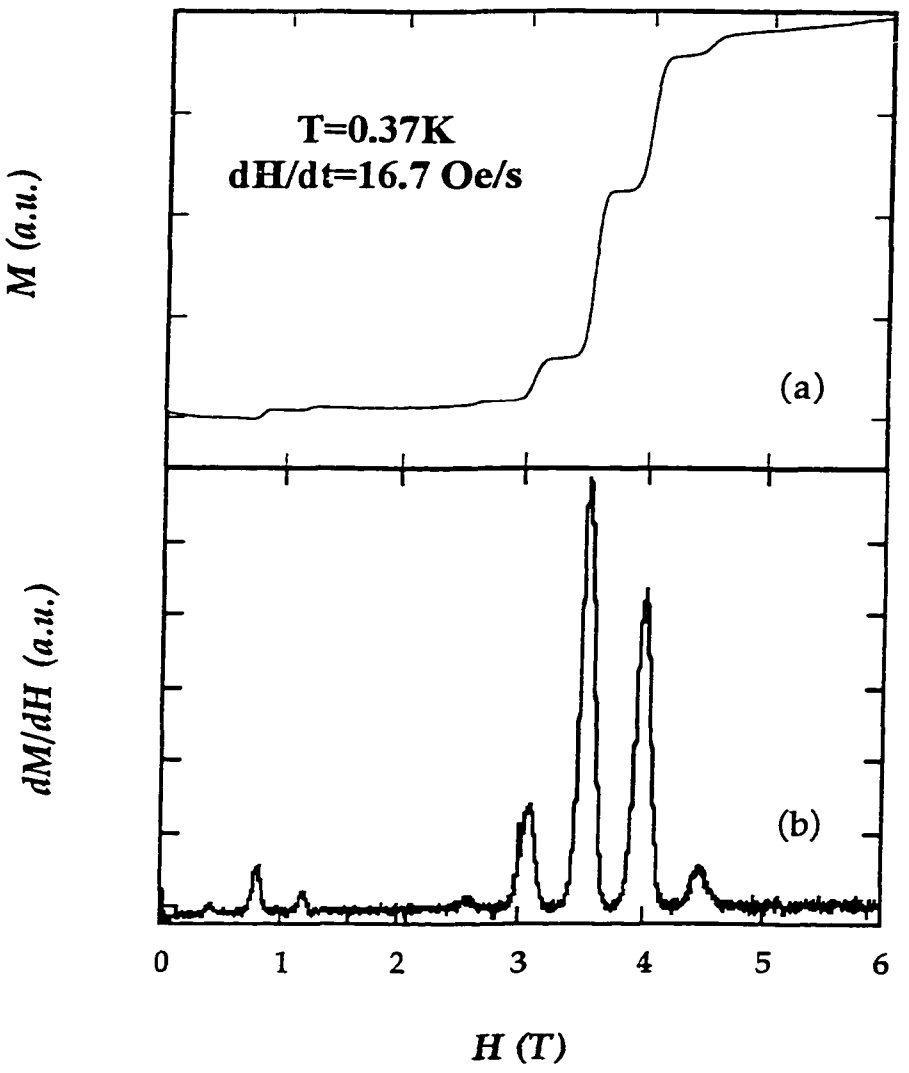

Figure 4.9: **Hysteresis curve of a Mn_{12} single crystal and its first derivative to magnetic field. Data was btained at 0.4 K and at field sweeping rate of 16.7 Oe/s**

amplitude.

The dependence of the dM/dH peaks on temperature is summarized in Fig. 4.11. Here the peak positons, in units of total field divided by the field quantum, H_0, are plotted versus temperature. Note that peaks initially shift gradually to higher magnetic field as the temperature is lowered. Between 0.6 K and 1.2 K the peak positions shift abruptly, with higher step indices changing position at lower temperature. The solid vertical line demarcates the approximate temperature at which these sudden shifts in step position occur. Below this line the step positions are independent of temperature.

4.3.2 Discussion

These experiments are the first to show that the steps in magnetization of Mn_{12} are not always at regular field interals and that steps shifts to higher magnetic fields as the temperature is lowered. This shift in peak position can be understood if we (again) take into consideration the fact that there are higher-order terms in the spin Hamiltonian (Eq. 2.2). The condition for level crossings is thus $H = NH_0(1 + A/D(m^2 + m'^2))$ and is no longer independent of m. Fields greater than NH_0 are necessary to bring low-lying magnetic sublevels into resonance, so that a shift in peak position to higher field signals a switch to tunneling from a state deeper in the potential well.

The physcal behaviour can be clearly distinguished in two different temperature regimes. At higher temperature (above the solid line in Fig. 4.11) the step positions shift gradually with temperature. This is the regime of thermally assisted tunneling,

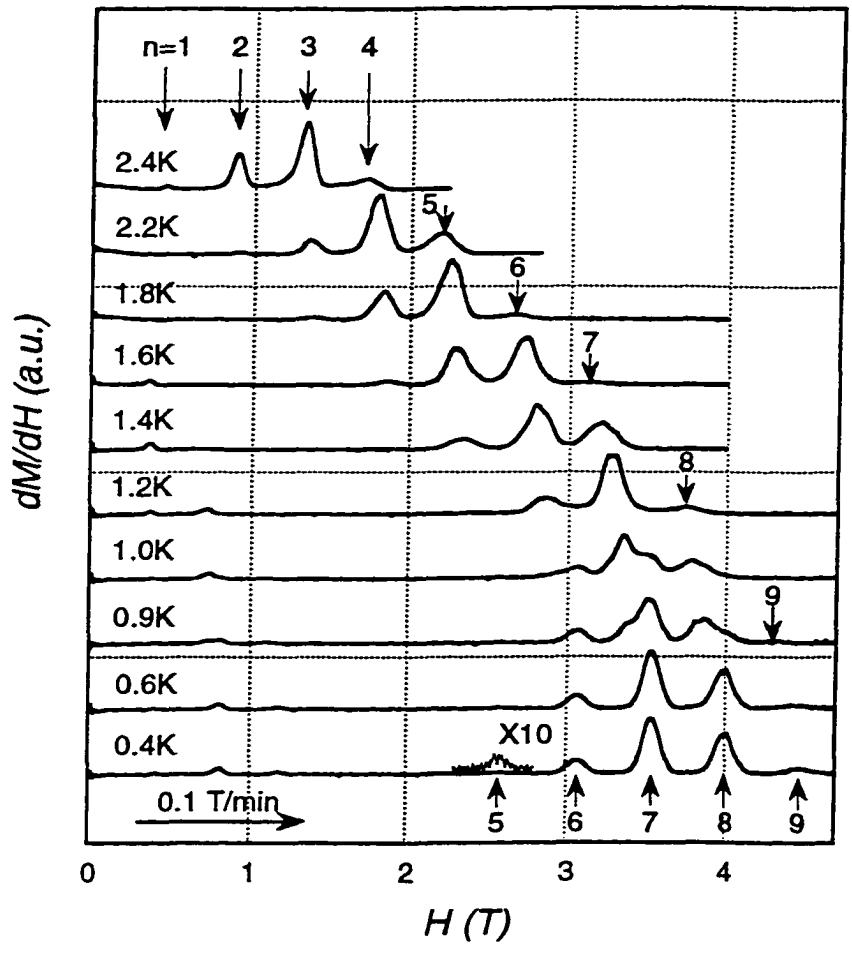

Figure 4.10: **First derivative to field of Mn_{12}'s hysteresis curves at ten temperatures. The field is applied along the easy magnetic axis (within a few degrees) and the field ramp rate is 0.1 T/min. The main figure shows the derivative of the magnetization with respect to applied field versus field at temperatures between 2.4 K and 0.4 K. Data are acquired from $M = 0$ at constant field ramp rate of 0.1 T/min. The small peaks at low temperature and fields ($H/H_o < 3$) are due to a small magnetic impurity phase in the crystal, discussed in reference [9]. Data near the $n = 5$ peak at 0.4 K is multiplied by 10 and offset so that it is visible on the plot.**

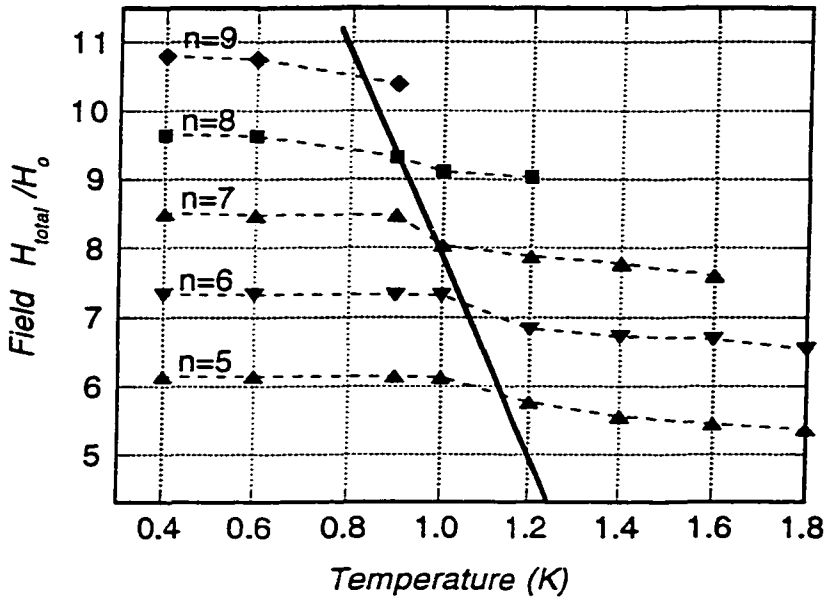

Figure 4.11: **Peak positions (from direvative of hysteresis curves) plotted as a function of temperature. Relaxation peak positions, $H_{total} = H + \alpha(4\pi M)$, normalized to H_o, the field quantum, versus temperature. The solid line shows the approximate temperature below which peak positions are temperature independent.**

where the magnetic escape is from thermally excited magnetic levels. We associate shifts in step positions with incremental changes in these levels, such as from m to $m-1$ (m negative), as the temperature is reduced and/or changes in the relative importance of a few levels, which contribute "in parallel" to the magnetization relaxation at a given temperature. Fig. 2.6 in Chapter 2 shows the enery levels versus field for the Mn_{12} spin Hamiltonian (Eq. 2.2). The solid lines indicate the level coincidences important to the magnetic relaxation in this temperature and field range. For example, for $N = 6$, the step positions we find are consistent with transitions from $m = -8$ to $m' = 2$ and $m = -7$ to $m' = 1$.

The second regime is at low temperature (below the solid line in Fig. 4.11) in which the position of peaks in dM/dH are independent of temperature. This is consistent with magnetization relaxation being of a pure quantum nature, i.e. tunneling escape occuring from the lowest level in the metastable well, $m = -10$. At 0.6 K and below, the amplitude of the peaks are also temperature independent. This is additional evidence for a quantum regime in Mn_{12}, as it indicates that the relaxation of the magnetization in the measurement time window has become temperature independent, therefore thermal excitations are no longer relevant to the relaxation.

A crossover to temperature-independent ground state tunneling has been observed in Fe_8 by Sangregorio *et al.* [13]. However, these experiments did not yield any information concerning the nature of this transition. It's important to note that our data provide a form of spectroscopy which allows a determination of which levels are involved in the tunneling.

The most striking feature of these data is the abrupt shift in step position, observed

at the boundary between these two regimes. This shift suggests that different levels become important to the tunneling relaxation in a narrow temperature interval. The shift in peak position in Fig. 4.11 is consistent with the change in levels responsible for tunneling illustrated by the dashed arrow in Fig. 2.6. m changes by 2 in an interval of 0.1 to 0.2 K. The abrupt nature of this transition is evident directly from the magnetic hystereis data in Fig. 4.11. For example, the shoulder which develops for the $n = 7$ peak at 2.0 K indicates that metastable levels $m = -8$ ($m' = 1$) and $m = -10$ ($m' = 3$) both contribute to the magnetic relaxation at this temperature but at different easy axis magnetic fields.

An interesting possibility is that the abrupt shift in peak position is evidence for a first-order transition between thermally assisted and pure quantum tunneling, as suggested recently by theory [14] (described in detail in Chapter 1). In this theory it is shown that for a small uniaxial magnetic particle the energy of the quasilevels in the metastable magnetic well which dominate the magnetic escape need not be a smooth function of temperature. For small transverse field, Chudnovsky and Garanin find that the transition can be first-order with certain energy levels in the metastable well being skipped entirely as the temperature is varied. Further solid experimental evidence has been obtained to support the abrupt nature of this transition [60].

Chapter 5

The Effect of a Transverse Magnetic Field on the Lineshape of the $N = 0$ Resonance

Previous chapters (2-4) all have one thing in common: they are centered around the key experimental fact that there is a substantial higher-order uniaxial anisotropy. In this chapter, I will deviate a little bit from this major theme of my thesis to present data from relaxation measurements performed for a narrow range of longitudinal magnetic fields around the $H = 0$ resonance (i.e. around the resonance of "step number" $N = 0$) in fixed transverse magnetic fields between 0 and 800 Oe. Interesting effects from such a transverse field on tunneling were observed. These results will be discussed in light of our current understanding of tunneling in Mn_{12}.

5.1 Motivations for this study

The effect of a transverse magnetic field on the relaxation rate in Mn_{12} is one of the central questions in understanding the tunneling process in this material. From the spin Hamiltonian of Mn_{12}

$$\mathcal{H} = -DS_z^2 - \mu_B \mathbf{H} \cdot \mathbf{g} \cdot \mathbf{S} - AS_z^4 + C(S_+^4 + S_-^4) \tag{5.1}$$

it can be seen that a Zeeman term due to transverse field $-g_x \mu_B H_x S_x$ and a higher order transverse anisotropy $C(S_+^4 + S_-^4)$ are the two possible symmetry-breaking terms that drive tunneling. Of these two, only the transverse magnetic field can be tuned experimentally to change the tunneling rate in Mn_{12}. Experimentally, the effect of a transverse magnetic field on resonant magnetization tunneling in Mn_{12} has been studied by Friedman *et al.* [23], who found through hysteresis measurements that the positions of the resonances is independent of the transverse component of the field, and is determined solely by the longitudinal component. On the other hand, it was shown that a transverse magnetic field significantly increases the relaxation rate, both on and off resonance for the $N = 1$ resonance. Theoretically, Garanin and Chudnovsky [32] developed a model for thermally-assisted tunneling in Mn_{12} based on such a symmetry-breaking transverse field term and their theory predicts some very interesting behavior as a function of transverse field, such as a change from a first-order to a second-order transition between thermally-activated relaxation and pure tunneling, as we discussed in detail in Chapters 1 and 4.

The experiment to be discussed was motivated by several issues. First, it was suggested by several authors [31, 32], that the transverse component of a weak internal magnetic field due to hyperfine and/or dipolar field, estimated at several hundred Oe, provides the necessary tunnel splitting to drive tunneling even in the absence of any external magnetic field (i.e. for resonance $N = 0$). If this situation holds

true, then by applying externally a pure transverse field to Mn_{12}, we should observe that the relaxation rate remains roughly the same when the external field is only a fraction of the internal field, and then goes through a crossover until finally the external field completely dwarfs the internal one, and the rate should then rise sharply. This reasoning needs to be tested for the zero field resonance, and the experiment would also yield information concerning the size of the internal field. Second, the $N = 0$ resonance is a special resonance that requires extra attention. *All* pairs of levels come into resonance simultaneously *only* in the case of $N = 0$ when the double well potential is symmetric[1]. Furthermore, in contrast with transverse field relaxation measurements on the odd-numbered $N = 1$ resonance, which were carried out in the experiment mentioned above [23], this experiment deals with an even numbered resonance. Differences associated with the tetragonal symmetry of Mn_{12} can be expected for these two types of resonances due to the transverse anisotropy term in the Hamiltonian written above.

5.2 Experimental Procedure

Millimeter sized single crystal samples were prepared according to the published procedure [7]. Measurements of the dc magnetization were performed using a Quantum Design MPMS-5 magnetometer equipped with a 5.5 Tesla superconducting magnet. The single crystal samples were mounted on a Quantum Design horizontal sample rotator, which allowed rotation of the easy axis of the single crystal sample with respect to the field in increments as small as 0.1 degrees. Two separate SQUIDs measured

[1]This situation is not true for nonzero step numbers and it constitutes the basis for all work presented in earlier chapters.

the sample's magnetization both parallel and perpendicular to the field direction, and the magnetization along the easy axis was inferred from these two orthogonal components.

The c-axis of the single crystal was first aligned parallel to a field of 1 kOe at 5 K by minimizing the magnetization perpendicular to that field. This step serves as a reliable starting point for later angular rotation. The sample was then cooled in zero magnetic field to 2.60 K. It was then immediately rotated to make an angle θ between the field direction and the c-axis. A magnetic field of appropriate magnitude was then quickly applied. (The desired values of the longitudinal and transverse field components were set by carefully choosing the angle between the field and the sample's c-axis.) The magnetic relaxation was measured (each curve taking up to four hours) and a relaxation rate was obtained from the long-time part of relaxation[2].

The same measurement procedure was repeated for other pairs of longitudinal and transverse field values. Since this experiment is focussed on studying the $N = 0$ resonance, relaxation rates in a *narrow* range of longitudinal magnetic fields around $H = 0$ were measured for fixed transverse fields up to 800 Oe.

5.3 Results and Discussions

The relaxation rate as a function of the longitudinal magnetic field at zero transverse field was remeasured in this experiment with a single crystal sample and the result is shown in Figure 5.1. The overall lineshape can be fit very well by a Lorentzian function, confirming an earlier experiment by Friedman *et al.* [35] using well-oriented

[2]There is a faster-than-exponential relaxation in the first 2000 seconds which is not included in the exponential fit to obtain the rate [19, 35]

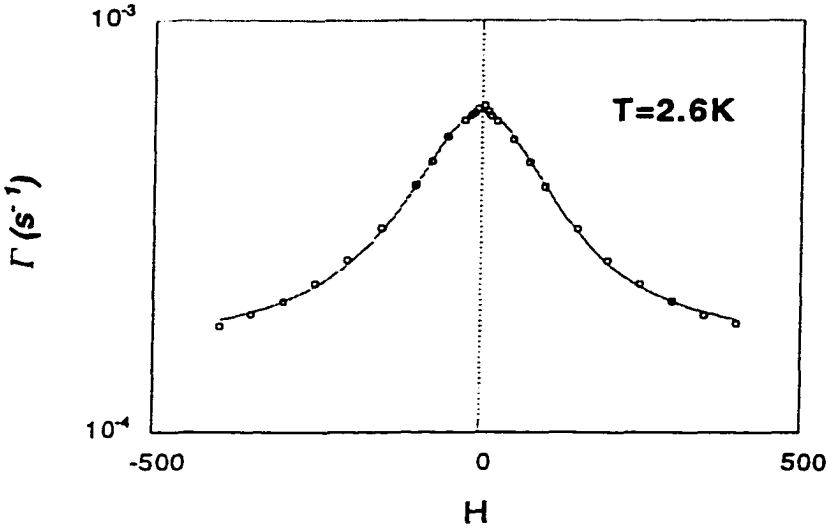

Figure 5.1: **Lorentzian fit of lineshape for the N=0 reseonance at $H_t = 0$. The near perfect fit to a Lorentzian function seriously contradicts the proposition that random hyperfine fields in Mn_{12} are responsible for broadening of resonances.**

Mn_{12} powder.

The lineshape in the presence of a transverse magnetic field is shown in Figure 5.2, where relaxation rates at six progressively higher transverse fields from 0 to 800 Oe are plotted as a function of the longitudinal field. The main features of the data can be summarized as follows:

First, in the presence of small transverse magnetic fields up to about 300 Oe, the relaxation rate remains roughly constant over the whole range of longitudinal field shown in this plot. (Please note the data points nearest to the center of the resonance are at $H_z = \pm 25$ Oe.) Second, the relaxation rate increases dramatically for fields above 500 Oe. Interestingly, this increase is only reflected within a narrow range of 100 Oe very near the center of the resonance. Third, the relaxation rate increases

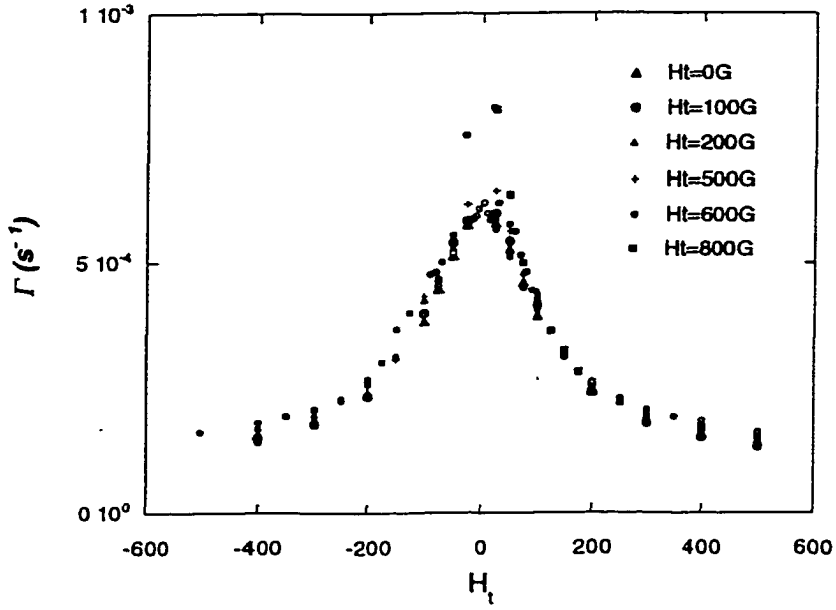

Figure 5.2: **H=0 resonance lineshapes at six different transverse fields.**

very little in a wide range of longitudinal fields far from the center of the resonance. Phenomenologically, the whole lineshape can be seen as consisting of two parts: The first is a broad "background" which is insensitive to the increase of the transverse field (at least when it is below 800 Oe, the highest transverse field applied in this experiment), while the second part only changes the line within a narrow range of about 100 Oe near the center of the resonance. The change near the center of the resonance is quite large for transverse fields above about 500 Oe.

Let us now briefly review the lineshape experiment of Friedman *et al.* [35] and the intriguing questions it raised, as discussed in Chapter 1. I will then attempt to gain further insight into the problem through our data. As pointed out by Friedman *et al.*, the high quality fit of the lineshape to a Lorentzian instead of a Gaussian function at *zero* transverse field makes it very difficult (if not impossible) to attribute the overall lineshape to broadening from a hyperfine field, which is known to fluctuate randomly

both in space and time, since a field of this nature should yield homogeneous (or Gaussian-shaped) broadening. Intuitively, the observed resonance lineshape $\Gamma(H_z)$ represents a distribution of the longitudinal component of the internal field within the Mn_{12} molecules which should be Gaussian according to basic probability laws. This quantitative difference between theory and experiment prompted these authors to conclude that the tunneling mechanism in Mn_{12} is far from understood.

In a way, the data presented in this chapter escalates the above quantitative difference into a sharp contradiction. The application of a well-controlled external transverse field to the $N = 0$ resonance adds a new dimension to this problem. First, let's look at the broad feature since it basically represents the Lorentzian-like background. (Please note that in this part of lineshape, the difference between high transverse fields and zero transverse field is very small. And we now know that lineshape at zero transverse field is a Lorentzian.)

If the hyperfine field, estimated at 300-500 Oe[33], were responsible for broadening of this order, then the application of a transverse magnetic field of 800 Oe (nearly twice the value of the estimated hyperfine field) would be expected to have a measurable effect on the tunneling rate. Our conclusion therefore is that the observed lineshape is not due to the random fluctuating internal hyperfine field. Other possible sources, such as spin-phonon interaction, are possible candidates for the observed broad structure.

Let us then focus our attention on the dramatic increase of the relaxation rate near the center of the resonance when the transverse field is above a threshold value of about 500 Oe. In the high temperature regime (2.60 K in our experiment) magnetization tunneling in Mn_{12} is thermally assisted. It is very likely that two or more tunneling channels contribute in parallel to the spin reversal. Let us assume that tunneling occurs mostly through the $m = \pm 3$ channel in the absence of an external

transverse field at 2.60 K, and tunneling relaxation via the $m = \pm 4$ channel is relatively small by comparison. However, when a large enough transverse field is applied, the tunnel splitting between the lower level pairs becomes large and this lower channel will essentially be "unfrozen" and become a prominent tunneling channel with a sharp increase in resonant relaxation rate.

Several theoretical works have suggested a picture similar to the observations in this experiment. Using a "basic" spin Hamiltonian of the form

$$\mathcal{H} = -DS_z^2 - H_z S_z - H_x S_x, \tag{5.2}$$

Garanin and Chudnovsky [32] calculated the biased-field dependence of the resonant tunneling escape rate of the uniaxial spin model at progressively higher transverse magnetic field. Their results reveal that in the nearly unbiased case (or $N = 0$), a *new narrow peak* corresponding to lower level tunneling emerges as H_x increases. Another calculation by Friedman [19] using a phenomenological microscopic model to describe the dynamics of spin reversal in Mn_{12} found that an increasing transverse field can cause successive sharp peaks to appear at the center of the resonance as the old peak broadens to join a uniform background. Each new peak in this calculation corresponds to a subsequently lower level which comes into play in the tunneling process. A detailed quantitative analysis of the data is required to determine whether this model can account for our results.

To summarize, in agreement with earlier results by Friedman *el al.* [35], this experiment further demonstrates that the broad lineshape *cannot* be explained as the result of a fluctuating internal hyperfine field since the application of an external transverse field (about twice the estimated internal field) has little influence on it. The most intriguing result is that the central portion of of the lineshape rises sharply when the transverse field is above about 500 Oe. This behavior may be due to the onset of tunneling from the next lower level in the double well potential. A quantitative

comparison is required to determine whether this explanation is correct.

Chapter 6

Ideas for Future Research and Summary

Intensive research activity has proceeded in the field of Quantum Tunneling of Magnetization during the past five years, and it will certainly continue before the unanswered central problems in this field are solved successfully. In this chapter, I will make an attempt to look into the future of this field to present a few ideas for continuing research. I will then close the dissertation with a summary of what has been accomplished.

6.1 Ideas for Future Research

As discussed in the last chapter, the application of micron-scale Hall-effect magnetometry to the study of magnetic relaxation opens up a wide range of field and temperature in which magnetization tunneling can be studied in great detail. It is particularly advantageous to use this technique if we want to make relaxation stud-

ies in the presence of a large magnetic field (of several tesla). It is expected that a more detailed relaxation study can be done in the low temperature regime (below 1 K) in which pure quantum tunneling gradually takes over with a decrease of temperature. Specifically, the following experiments can be performed to gain further understanding of tunneling relaxation in Mn_{12}.

It is desirable to study magnetic relaxation in Mn_{12} relaxation in the high longitudinal field, low temperature regime (with or without external transverse magnetic field). In this regime, the double well potential is substantially tilted and the tunneling is purely out of the ground state in the metastable well. The time scale of this pure tunneling relaxation nevertheless can still match the measurement time if we carefully choose the combination of field and temperature. Performing relaxation studies in this regime around one of the higher "step number" resonances (e.g. $N = 7$ or 8) can provide valuable information on the magnetic relaxation law and the relaxation lineshape in this regime for Mn_{12}. It is known from early studies that the magnetic relaxation in Mn_{12} between 2 and 3 K is exponential at long times. However, preliminary results from some authors found non-exponential decay at much lower temperatures. Since non-exponential decay signals the breakdown of magnetically independent spin reversal of identical Mn_{12} clusters within a single crystal, these results need to be checked. Another point is closely related to our discussion in the chapter on the effect of a transverse field on the $N = 0$ resonance lineshape. We noted that there is a broad feature which is insensitive to the transverse field. It will be very interesting to see how the important features for the relaxation lineshape (width, curve shape) will change for the $N = 7$ and 8 resonances at much lower temperatures. This should help gain further insight into the Lorentzian lineshape puzzle.

Since the tunneling of the magnetization proceeds from the ground state in the metastable well in this temperature regime, the measured relaxation rate only re-

flects tunneling escape from *one* level instead of several levels contributing in parallel. Therefore it would be much more straightforward to compare experimental data to theoretical calculations for this system. In addition, it will also be more direct to observe the effect of a transverse field applied to a Mn_{12} single crystal around one of its high indexed resonances.

Furthermore, the small size of a Hall bar plate (typically 1×1 cm^2) enables it to be placed into a small space where microwave excitation is generated. It has been suggested by many authors that the inter-well relaxation rate in Mn_{12} can be substantially altered if microwave of appropriate frequencies is applied to the system. The high sensitivity and fast response of a Hall probe makes it a good magnetization recorder in the microwave environment. This is a very interesting experiment that needs to be performed.

6.2 Summary

In this dissertation, I have presented three types of experimental data from several experiments which show deeper and richer behavior of the Mn_{12} system. The first type, inelastic neutron scattering study, provides an accurate energy level scheme of the Mn_{12} spin-10 system and establishes the existence of higher order uniaxial anisotropy in Mn_{12}. The second type of experiments consists of two magnetic relaxation experiments — the relaxation rate as a function of only externally applied longitudinal magnetic field and as a function of transverse field near the $N = 0$ resonance. The first experiment corroborated the existence of the higher order term but raises some unresolved puzzles related to the so-called "odd-even asymmetry" in the relaxation rate. The latter experiment supports ealier observations of Friedman *et al.*

that the lineshape of the resonance in Mn_{12} is not well understood, and adds some very intriguing features in the form of a sharp increase only at the center the $N = 1$ resonance when the transverse field is above 500 Oe. Finally, a large portion of this thesis is devoted to measurements using micron-scale Hall-effect magnetometry at very low tempertures. The dramatic shift of peak positions in the hysteresis curves with decreasing temperature provides evidence in support of theoretical predictions of a first-oder transition in the escape rate in spin systems. I expect future experimental work will further benefit from the nice tool of Hall magnetometry and also hope more flourishing theoretical works will come out to challenge us (as experimentalists).

Bibliography

[1] A. O. Caldeira and A. J. Leggett, Phys. Rev. Lett. **46**, 211 (1981).

[2] A. J. Leggett, S. Chakravarty, A. T. Dorsey, M. P. A. Fisher, A. Garg, and W. Zwerger, Rev. Mod. Phys. **59**, 1-85 (1987).

[3] U. Weiss, H. Grabert, and S. Linkwitz, J. Low Temp. Phys. **68**, 213 (1987).

[4] E. M. Chudnovsky and L. Gunther, Phys. Rev. Lett. **60**, 661 (1988).

[5] D. D. Awschalom and D. P. Di Vincenzo, Phys. Today **48** (4), 42 (1995).

[6] L. Gunther, in *Quantum Tunneling of Magnetization*, edited by L. Gunther and B. Barbara (Kluwer, Amsterdam, 1995), p. 413.

[7] T. Lis, Acta Cryst. B **36**, 2042 (1980).

[8] K. Wiedghardt, K. Pohl, J. Jibril, and G. Huttner, Angew. Chem. Int. Ed. Engl. **23**, 77 (1984).

[9] W. Wernsdorfer, R. Sessoli, and D. Gatteschi, Europhys. Lett., **47**, 254 (1999).

[10] J. R. Friedman, M. P. Sarachik, J. Tejada, and R. Ziolo, Phys. Rev. Lett. **76**, 3830 (1996).

[11] M. A. Novak and R. Sessoli, in *Quantum Tunneling of Magnetization*, (Kluwer, Amsterdam, 1995).

[12] L. Thomas, F. Lionti, R. Ballou, R. Sessoli, D. Gatteschi, and B. Barbara, Nature (london) **383**, 145 (1996).

[13] C. Sangregorio, T. Ohm, C. Paulsen, R. Sessoli, and D. Gatteschi, Phys. Rev. Lett. **78**, 4645 (1997).

[14] E. M. Chudnovsky and D. A. Garanin, Phys. Rev. Lett. **79**, 4469 (1997).

[15] A. Caneschi, D. Gatteschi, R. Sessoli, A. L. Barra, L. C. Brunel, and M. Guillot, J. Am. Chem. Soc. **113**, 5873 (1991).

[16] R. Sessoli, H.-L. Tsai, A. R. Schake, S. Wang, J. B. Vincent, K. Folting, D. Gatteschi, G. Christou, and D. N. Hendrickson, J. Am. Chem. Soc. **115**, 1804 (1993).

[17] C. Paulsen, J.-G. Park, B. Barbara, R. Sessoli, and A. Caneschi, J. Magn. Magn. Mater. **140-144**, 379 (1995).

[18] M. A. Novak, R. Sessoli, A. Caneschi, and D. Gatteschi, J. Magn. Magn. Mater. **146**, 211 (1995).

[19] Jonathan R.Friedman, Ph.D. Thesis, The City University of New York (1996).

[20] F. Fominaya, J. Villain, P. Gandit, J. Chaussy, and A. Caneschi, Phys. Rev. Lett. **79**, 1126 (1997).

[21] A. M. Gomes, M. A. Novak, R. Sessoli, A. Caneschi, and D. Gatteschi, Phys. Rev. B **57**, 5021 (1998).

[22] F. Luis, J. Bartolomé, J. F. Fernández, J. Tejada, J. M. Hernández, X. X. Zhang, and R. Ziolo, Phys. Rev. B **55**, 11448 (1997).

[23] Jonathan R. Friedman, M. P. Sarachik, J. M. Hernandez, X. X. Zhang, J. Tejada, E. Molins, and R. Ziolo, J. Appl. Phys. **81**, 3978 (1997).

[24] A. L. Barra, D. Gatteschi, and R. Sessoli, Phys. Rev. B **56**, 8192 (1997).

[25] S. Hill, J. A. A. J. Perenboom, N. S. Dalal, T. Hathaway, T. Stalcup, and J. S. Brooks, Phys. Rev. Lett. **80**, 2453 (1998).

[26] S. Hill *et al.*[25] considered fourth order terms of the form $[D_{4||} \times S_z^4 + D_{4\perp} \times (S_x^4 + S_y^4)]$ and set $D_{4||} = D_{4\perp}$.

[27] M. Hennion, L. Pardi, I. Mirebeau, E. Suard, R. Sessoli, and A. Caneschi, Phys. Rev.B **56**, 8819 (1997).

[28] P. A. Langan , R. A. Robinson, P. J. Brown, D. N. Argyriou, D. N. Hendrickson, and S. M. J. Aubin, 2000 J. Phys. Chem. submitted. This structure has also been deposited in the Cambridge Structural Data base under entry CCDC114737.

[29] R. A. Robinson, P. J. Brown, D. N. Argyriou, D. N. Hendrickson, and S. M. J. Aubin, J. Phys.: Condens. Matter. **12** 2805 (2000).

[30] D. A. Garanin, J. Phys. A: Math. Gen. **24**, L61 (1991).

[31] J. M. Hernández, X. X. Zhang, F. Luis, J. Tejada, J. R. Friedman, M. P. Sarachik, and R. Ziolo, Phys. Rev. B **55**, 5858 (1997).

[32] D. A. Garanin, E. M. Chudnovsky, Phys. Rev. B **56**, 11102 (1997).

[33] F. Hartmann-Boutron, P. Politi, and J. Villain, Int. J. Mod. Phys. **10**, 2577 (1996).

[34] A. Caneschi, T. Ohm, C. Paulsen, D. Rovai, C. Sangregorio, and R. Sessoli, J. Magn. Magn. Mater. **177**, 1330 (1998).

[35] Jonathan R. Friedman, M. P. Sarachik, and R. Ziolo, Phys. Rev. B **58**, R14729 (1998).

[36] A. Fort, A. Rettori, J. Villain, D. Gatteschi, and R. Sessoli, Phys. Rev. Lett. **80**, 612 (1998).

[37] F. Luis, J. Bartolomé, and J. F. Fernández, Phys. Rev. B **57**, 505 (1998).

[38] M. N. Leuenberger and D. Loss, Europhys. Lett. **46**, 692 (1999).

[39] T. Pohjola and H. Schoeller, preprint cond-mat/0005135 (2000).

[40] R. Sessoli, D. Gatteschi, A. Caneschi, and M. A. Novak, Nature (London) **365**, 141 (1993).

[41] C. Paulsen, J.-G. Park, B. Barbara, R. Sessoli, and A. Caneschi, J. Magn. Magn. Mater. **140-144**, 1891 (1995).

[42] A. I. Larkin, Y. N. Ovchinnikov, Sov. Phys. JETP **59**, 420 (1984).

[43] D. A. Garanin, X. Martínez Hidalgo, and E. M. Chudnovsky, Phys. Rev. B **57**, 13639 (1998).

[44] D. A. Garanin and E. M. Chudnovsky, Phys. Rev. B **59**, 3671 (1999).

[45] W. Wernsdorfer, E. Bonet Orozco, K. Hasselbach, A. Benoit, B. Barbara, N. Demoncy, A. Loiseau, H. Pascard, and D. Mailly, Phys. Rev. Lett. **78**,1791 (1997).

[46] J. A. A. J. Perenboom, J. S. Brooks, S. Hill, T. Hathaway, and N. S. Dalal, Phys. Rev. B **58**, 330 (1998).

[47] E. M. Chudnovsky and J. Tejada, *Macroscopic Quantum Tunneling of the Magnetic Moment*, Cambridge University Press, 1998.

[48] N. V. Prokof'ev and P. C. E. Stamp, Phys. Rev. Lett. **80**, 5794 (1998).

[49] W. Wernsdorfer, T. Ohm, C. Sangregorio, R. Sessoli, D. Mailly, and C. Paulsen, Phys. Rev. Lett. **82**, 3903 (1999).

[50] L. Thomas, A. Caneschi, and B. Barbara, Phys. Rev. Lett. **83**, 2398 (1999).

[51] W. Wernsdorfer, R. Sessoli, and D. Gatteschi, Europhys. Lett. **47**, 254 (1999).

[52] G. L. Squires, Introduction to the Theory of Thermal Neutron Scattering, Cambridge University Press, 1978.

[53] K. F. Bradley, S-H Chen, T. O. Brun, R. Kleb, W. A. Loomis, and J. M. Newsam, Nuclear Instruments and Methods in Physics Research, **A270**, 78-89(1988).

[54] R. Sessoli, H-L Tsai, A. R. Schake, S. Wang, J. B. Vincent, K. Folting, D. Gatteschi, G. Christou, and D. N. Hendrickson, J. Am. Chem. Soc. **115**, 1804 (1993).

[55] M. I. Katsnelson, V. V. Dobrovitski, and B. N. Harmon, Phys. Rev. B **59**, 6919 (1999).

[56] I. Mirebeau, M. Hennion, H. Casalta, H. Andres, H. U. G'udel, A. V. Irodova, and A. Caneschi, Phys. Rev. Lett. **83**, 628 (1999).

[57] A.D. Kent, S. V. Molnar, S. Gider, and D. D. Awschalom, J. Appl. Phys. **76**, 6656 (1994).

[58] E. Zeldov, D. Majer, M. Konczykowski, V. B. Geshkenbein, V. M. Vinokur, and H. Shtrikman, Nature **375**, 373 (1995).

[59] C. Paulsen, J.-G. Park, in *Quantum Tunneling of Magnetization* (Dordrecht, Kluwer, 1995).

[60] K. M. Mertes, Yicheng Zhong, M. P. Sarachik, Y. Paltiel, H. Shtrikman, E. Zeldov, E. Rumberger, D. N. Hendrickson, preprint, October 2000.